Inactivation effects of plasma-activated water on *Fusarium graminearum*

Jian Guo[a], Jiaoyu Wang[b], Hui Xie[a], Junlong Jiang[a], Chunyuan Li[a], Wanting Li[a], Ling Li[a*], Xingquan Liu[a], Fucheng Lin[b, c]

[a] College of Agriculture and Food Science, Zhejiang Agriculture & Forestry University, No. 666 Wusu Street, Hangzhou 311300, China

[b] State Key Laboratory for Managing Biotic and Chemical Treats to the Quality and Safety of Agro-products, Institute of Plant Protection and Microbiology, Zhejiang Academy of Agricultural Sciences, Hangzhou 310021, China

[c] Institute of Biotechnology, Zhejiang University, Hangzhou, 310058, China

Abstract

The continuous usage of fungicides poses a potential threat to the environment, ranging from mere irritation to being very toxic to human beings and organisms. Plasma-activated water (PAW) has recently gained much interest as a promising candidate to inactivate fungi. However, the inactivation mechanisms of PAW are still not well understood. In this study, the effect of PAW on the viability and the cellular responses of *Fusarium graminearum* in PAW inactivation were investigated. The results showed that microbial activity of spores was significantly inhibited by PAW treatment ($P < 0.05$). The symptoms caused by *F. graminearum* were significantly reduced on the spikelets. Our data indicated that PAW could induce cell wall sculpturing, membrane permeability changes, and mitochondrial dysfunction. Differential gene expression analysis also confirmed that the cell membrane, the cell wall and the

* Corresponding author.

E-mail: liling-06@163.com

mitochondria were the organelles most affected by PAW. The results from this study facilitate the understanding of the mechanisms underlying the responses of *F. graminearum* to PAW and the development of PAW as a potential fungicidal agent or an effective supplement to fungicides.

Keywords Inactivation mechanism; Pathogen; Reactive oxygen species; Eco-friendly fungicide; Differential gene expression

1. Introduction

Phytopathogens are the main causes of plant diseases, they significantly reduce the yield of agricultural crops (McMullen et al., 1997; Marcos et al., 2008). The use of fungicides in modern agricultural practices has made crop production stable, and environmental and food safety issues associated with the use of fungicides cannot be ignored. Prolonged or repeated application of agricultural chemicals has led to the outbreak of acute or chronic diseases, toxicity to nontarget organisms, excessive fungicide residues, and groundwater and surface water contamination (Pimentel et al., 1992; Soylu et al., 2010). *Fusarium graminearum* is an ascomycetous fungus that is the major cause of *Fusarium* head blight (FHB) on wheat and barley, as well as stalk and ear rot disease on maize. This fungus not only causes crop yield and quality losses but also contaminates grain with mycotoxins, rendering them unfit for food or feed (Etzerodt et al., 2016; Kim and Vujanovic, 2016; Masci et al., 2015; Zhou et al., 2021). Benzimidazoles and sterol demethylation inhibitors are widely used for the control of FHB (Blandino et al., 2006; Bian et al., 2021). However, these synthetic chemicals are difficult to degrade and are harmful to the environment and human health (Zheng et al., 2019). Therefore, much attention has been given to the development of highly efficient, environmentally friendly, and low-residue novel antifungal agents.

Cold plasma is an electrically energized matter in a gaseous state that is composed of charged particles, free radicals, and some radiation. To obtain cold plasma, an electrical discharge device is needed, which is not convenient for practical applications. Plasma treatment of water, termed plasma-activated water (PAW), alters the physicochemical properties of water, such as the redox potential, pH and conductivity. As a result, PAW has a different chemical composition than water and can serve as an alternative method for microbial disinfection (Ercan et al., 2013; Guo et al., 2021; Natali et al., 2010;

Oehmigen et al., 2010; Puligundla et al., 2018; Shen et al., 2016; Traylor et al., 2011; Tian et al., 2015; Xiang et al., 2019a; Xu et al., 2020; Zhang et al., 2016). Reactive oxygen and nitrogen species (RONS) are the major agents for air-plasma-induced biological effects, and almost no harmful byproducts are generated in the plasma treatment process (Xu et al., 2020). In our previous study, the oxidative stress and acidity of PAW were not persistent (Guo et al., 2017; Guo et al., 2021; Shen et al., 2016). The lifetime of the chemical components in PAW is short and labile (Brisset et al., 2011; Girard et al., 2016; Pavlovich et al., 2013), and it leaves less residue and harmful chemical components on crops than conventional approaches. Thus, PAW can be regarded as a promising eco-friendly approach for fungal inactivation.

Previous studies have showen that chemical components generated in PAW and the oxidative stress it induces play major roles during PAW treatments (Natali et al., 2010; Oehmigen et al., 2010; Pavlovich et al., 2013; Zhang et al., 2013). It is generally accepted that different plasma devices and working gases could lead to different inactivation efficiencies and inactivation patterns. For instance, oxygen-containing gases can increase the proportion of reactive oxygen species (ROS) leading to a higher inactivation efficiency. It was also found that ROS play an important role in direct plasma inactivation in an aqueous environment (Chandana et al., 2018; Gorbanev et al., 2018; Guo et al., 2021; Xu et al., 2020). Kaneko et al. (2017) found that ·OH plays a key role in gas-liquid interfacial plasma irradiation. Xu et al., (2020) reported that $^1O_2$ contributes the most to the yeast cells. Because of the complexity of the reactive species in plasma and the different roles played by short- and long-lived ROS, the cold plasma inactivation mechanisms caused by these RONS in an aqueous environment or PAW are not yet fully understood.

Apart from the different roles played by the diverse reactive species in the cold plasma inactivation process, the complexity of the antimicrobial mechanisms of PAW is also attributed to the complicated cellular response. Many works have found that different types of microorganisms have different

responses to cold plasma treatment or PAW treatment. Many works have reported that different types of microorganisms behave differently in their interactions with RONS in cold plasma or PAW. Xiang et al. (2019b) found that gram-negative *E. coli* bacteria were more sensitive to PAW than the gram-positive *S. aureus* bacteria, which might be due to the significant differences in the cell wall structures of gram-negative and gram-positive bacteria, especially the thickness of the peptidoglycan layer. Han et al. 2016 reported that cold plasma inactivated *E. coli* mainly through damaging the cell wall, while *S. aureus* was inactivated by cold plasma primarily through damaging the intracellular components. Furthermore, it is commonly considered that fungal resistance against cold plasma is generally higher than that in bacteria due to the complex cell wall structure and specialized cellular organelles (such as mitochondria and ribosomes) (Xu et al., 2020). The cell wall of fungi consists of chitin, which is more rigid than the peptidoglycan of bacterial cell walls. Lunov et al. (2016) reported that plasma could induce two different inactivation mechanisms (apoptosis or direct physical destruction) in bacteria depending on the plasma treatment time. Xu et al. (2020) also revealed that yeast cells underwent apoptosis in the first 3 min of treatment due to the accumulation of intracellular ROS, mitochondrial dysfunction and intracellular acidification, followed by necrosis under longer exposure times, attributed to the destruction of the cell membrane. Itooka et al. (2018) revealed that cold plasma could cause protein denaturation and endoplasmic reticulum stress in *Saccharomyces cerevisiae*. However, studies that focus on the cellular responses in the PAW inactivation of fungi are very limited, especially from the perspective of gene expression.

In this work, the efficacy of PAW against *F. graminearum in vivo* and *in vitro* was first estimated by calculating the disease severity index and assessing the effects of PAW on mycelium growth, conidium germination and conidiation. The complicated cellular responses of *F. graminearum* to PAW

were explored by assessing cell morphology, cell membrane integrity, mitochondrial activity and gene expression.

2. Materials and methods

2.1. Fungal culture conditions

The *Fusarium graminearum* PH-1 strain used in this study was obtained from the Agricultural Culture Collection of China (Beijing, China). *F. graminearum* was aseptically inoculate in liquid complete medium (CM) at 30 °C for 7 d. The strain was routinely cultured on CM plates at 28 °C for mycelial growth assays. For the conidial germination assay, three mycelial plugs of the strain were inoculated in 30 mL of liquid CM under continuous light. After incubation in a shaker at 180 rpm at 28 °C for 7 d, conidia of each sample were collected by centrifugation and were quantified using a hemocytometer.

2.2. Plasma treatment system

The cold plasma device and operation method were described in our previous work (Guo et al., 2021). Sterile distilled water (200 mL) was activated by plasma treatment for 15, 30, 45 and 60 min. Accordingly, the samples after treatment were named as PAW15, PAW30, PAW45 and PAW60, and the control.

2.3. Physicochemical properties of PAW

To evaluate the physicochemical properties of PAW, the conductivity, oxidation reduction potential (ORP), and pH of PAW were all detected using a multimeter (Orion 3 Star pH/ORP Meter, Thermo

111 Fisher Scientific Inc, PA) immediately after production. ORP was used to estimate the oxidative stress
112 in PAW, the concentration of the oxidizers and their activity or strength (Mcferson, 1993).

113 The concentrations of nitrate anions (NO_3^-) and nitrite anions (NO_2^-) in PAW were determined by
114 spectrophotometry (Shen et al., 2016; Collos et al., 1999). Then, 50 mL of PAW was added to 1 mL of
115 1 M hydrochloric acid and 100 µl of 0.8% sulfamic acid. NO_3^- levels in PAW samples were determined
116 by ultraviolet absorption spectrometry (UV-1800, Shimadzu Corporation, Kyoto, Japan) at a single
117 wavelength of 220 nm.

118 For the determination of NO_2^-, sulphanilamide was used as the diazotizing reagent, and N-(1-
119 naphthy1)-ethylenediamine hydrochloride was used as the coupling reagent. After plasma activation, 1
120 mL of sulphanilamide solution (5 g of sulphanilamide was dissolved in a mixture of 50 mL of 37% (w/w)
121 concentrated HCl and 300 mL of water, and it was diluted to 500 mL with water) was added into 50 mL
122 of PAW, and incubated at room temperature for 2 min, subsequently adding 1 mL of 1.0 g L^{-1} N-(1-
123 naphthy1)-ethylenediamine hydrochloride at room temperature. After a 20-min incubation at room
124 temperature, the absorbance at 540 nm was measured using a spectrophotometer (UV-1800, Shimadzu
125 Corporation, Kyoto, Japan) for the determination of the concentrations of NO_3^- in the PAW.

126 *2.4. In vivo fungicidal activities assay*

127 The *in vivo* fungicidal activities of PAW against *F. graminearum* (strain PH-1) were evaluated as
128 follows: The spikelets were point-inoculated with 20 µl of the conidial suspension (10^5 conidia mL^{-1})
129 mixed with PAW. After inoculation, the spikelets were placed in a controlled chamber (90–100% relative
130 humidity, 22 °C) for 72 h. The disease severity was scored by measuring the lesion area with image
131 analysis software (ImageJ), and the disease severity index was calculated (the mean area of disease

132 divided by the total area of the wheat × 100%). The protection efficacies were calculated as follows:
133 Protection efficacy = [(mean area of infected spikelets of control – mean area of infected spikelets of
134 treated group)/mean area of infected spikelets of control] × 100%.

135 *2.5. In vitro fungicidal activities assay*

136 For the mycelium growth assay, 2 mL of PAW was transferred into the test tubes containing 0.5 mL
137 of *F. graminearum* spore suspension. After exposure for 1 h, 10 µl of *F. graminearum* spore suspension
138 was dropped at the center of CM or CR (Congo red was added to complete medium to 100 µg mL^{-1} or
139 200 µg mL^{-1}) and CFW (calcofluor white was added to complete medium to 50 µg mL^{-1}) plates. The agar
140 plates were incubated at 28 °C. Sterile water (2 mL) was used as the control. The colonial diameters of
141 the treated strain were carefully measured by a caliper, every 12 h over 5 d, and the inhibition ratios were
142 calculated using the following formulas:

143 $$I = \left(\frac{(D_c - D_t)}{D_c}\right) \times 100\% \quad (1)$$

144 where D_c and D_t are the colonial diameters of the control and treated groups, respectively.

145 The dry weight of the mycelial biomass was measured after 7 days of cultivation in liquid CR or
146 CFW medium.

147 Conidiation was assessed by growing the strain in liquid complete medium (CM) for 7 days. The
148 conidial concentration was measured using a hemocytometer.

149 For the conidial germination assay, spores from strain PH-1 were inoculated in the liquid CM in the
150 presence of PAW or were left untreated. PAW15, PAW30, PAW45 and PAW60 (0.4 mL) were
151 transferred into tubes that contained an *F. graminearum* spore suspension (0.1 mL), and the mixture was

allowed to stand for 1 h. Five microliters of the treated conidia was pipetted onto the concave slide at 25 °C for 6 h and then observed by fluorescence microscopy (Nikon Eclipse Ti-s; Tokyo, Japan) for the analysis of germ tube emergence. Sterile water (0.4 mL) was used as the control. Three different fields of view were observed randomly. The number of conidia observed in each test was at least 200. Although germ tube emergence marks the culmination of the germination process, it was used as a convenient marker for germination in our experiments (Semighini et al., 2008). The conidial germination ratios were calculated using the following formulas:

$$R = N_g / N_t \times 100\% \quad (2)$$

where R is the conidial germination ratio, N_g is the conidial germination number, and N_t is the conidial number.

The relative conidial germination ratios were calculated using the following formula:

$$R_e = R_t / R_c \times 100\% \quad (3)$$

where R_e is the relative conidial germination ratio, and R_t and R_c are the conidial germination ratios of the treated and control groups, respectively.

2.6. Effect of PAW on cell wall integrity

The effect of PAW on cell wall integrity was assayed by measuring the conidiation and dry mycelial weight of the strain grown in liquid CM supplemented with 100 mg L^{-1}, 200 mg L^{-1} Congo red and 50 mg L^{-1} Calcofluor White for 7 days.

2.7. SEM and TEM observations

To investigate the effect of PAW on the spore cell wall. We performed transmission electron

172 microscopy (TEM) imaging. After PAW treatment, the spores were fixed in Karnovsky's fixative (2%
173 v/v paraformaldehyde and 2% v/v glutaraldehyde in 1x PBS) overnight. The specimens were observed
174 using a Hitachi Model H-7650 TEM (Hitachi High-Tech Manufacturing & Service, Corp).

175 *2.8. Measurement of nucleic acid and protein leakage*

176 Spore cell membrane integrity was detected by determining the release of intracellular components
177 absorbing at 260 nm and 280 nm as described in the relevant literature (Cockrell et al., 2017; Xiang et
178 al., 2018) with slight changes. Spores were harvested by centrifugation at 5000 x g for 10 min at 4 °C,
179 and were then suspended in sterile deionized water. PAW15, PAW30, PAW45 and PAW60 were added
180 to spores suspensions. Spores treated with PAW0 were used as the control. To quantify the concentrations
181 of nucleic acids and proteins, the optical densities of the supernatants at 260 nm and 280 nm were
182 recorded.

183 *2.9. Measurement of mitochondrial activity and total microbial activity*

184 Spores were labeled with tetramethylrhodamine methyl ester (TMRM, 80 nM) for mitochondria
185 after PAW treatment. The cells were then washed three times and resuspended in PBS for observation.
186 Imaging of cells loaded with fluorescent dyes was performed using a Zeiss LSM510 system (Carl Zeiss,
187 Germany). The excitation wavelength was 543 nm and the emission was collected between 561 and 603
188 nm.

189 A stock solution of 500 μg mL^{-1} FDA was made in acetone and then diluted to 100 μg mL^{-1} in
190 incubation buffer. The cells were then washed three times and resuspended in PBS for observation.
191 Fluorescein was excited using a 488 nm laser, and the emission was collected between 505 and 530 nm.

2.10. RNAseq and transcriptomic analyses.

Fungal materials were frozen in liquid nitrogen and RNA was extracted using TRIzol® Reagent according to the manufacturer's instructions (Invitrogen), and genomic DNA was removed using DNase I (TaKaRa). The RNA-seq transcriptome library was prepared following the TruSeq™ RNA sample preparation kit from Illumina (San Diego, CA) using 1 μg of total RNA. After quantification by TBS380, the paired-end RNA-seq sequencing library was sequenced using an Illumina HiSeq xten/NovaSeq 6000 sequencer (2 × 150 bp read length). To identify DEGs (differentially expressed genes) between two different samples, the expression level of each transcript was calculated according to the fragments per kilobase of exon per million mapped reads (FRKM) method. RSEM was used to quantify gene abundances (Li and Dewey 2011). Differential gene expression analysis was performed with DESeq2 software based on negative binomial distribution.

2.11. Quantitative PCR

To evaluate the validation of RNA-seq transcriptome results, primers (Table 2) were designed for the following thirteen candidates selected based on the following criteria: the highest upregulated gene involved in mitochondrial function and the highest upregulated or the lowest downregulated gene involved in cell wall and membrane integrity. Quantitative PCR (Q-PCR) assays were conducted according to the relevant literature (Liu et al., 2010; Demissie et al., 2018) with slight changes. Normalized relative expression values ($\Delta\Delta C_T$) of the selected candidates were calculated using the formula $2^{-\Delta\Delta CT}$ (Livak and Schmittgen, 2001) using actin as a reference gene. Three amplifications were performed for each replicate. The expression of each tested gene in the PAW-treated sample relative to

that of the untreated sample was calculated according to the fragments per kilobase of exon per million mapped reads (FRKM) method.

2.12. Statistical analysis

Data from all experiments are expressed as the mean ± standard deviation (SD). At least three replicates were performed for each treatment condition. Statistical analysis was performed using Origin 2019b program. Analysis of variance (ANOVA) was used to calculate significant differences and to compare the means.

3. Results and discussion

3.1. Physicochemical properties of PAW

It is generally agreed that nitrate and nitrite usually exist in PAW generated by the air-cold plasma devices (Patangea et al., 2019; Pavlovich et al., 2013; Sarangapani et al., 2017). As shown in Fig. 1a, the concentrations of nitrate and nitrite in PAW increased significantly ($P < 0.05$) over air-plasma-activated time. Patangea et al. (2019) also reported that PAW generated using this submerged DBD air-plasma device contained high concentrations of nitrate but a very low concentration of nitrite. When the discharge area is above the liquid surface, similar amounts of nitrate and nitrite were generated in the PAW using this type of cold plasma device (Pavlovich et al., 2013; Sarangapani et al., 2017). When the discharge area is below the water surface, there are more changes for the oxygen or ROS in air plasma to oxidize the nitrite in PAW. Therefore, most nitrite in the PAW generated using a submerged DBD air-plasma device is transformed into nitrate (Guo et al., 2021).

ORP reveals the total oxidation ability of various substances in a solution, and is an important

232 indicator in water disinfection applications because there is a direct correlation between high ORP and
233 cell membrane damage (Ma et al., 2015; Tian et al., 2015; Xiang et al., 2018). As shown in Fig. 1b, the
234 ORP of water after plasma activation increased from 235.8±5.43 mV to 394.9±23.69 mV, and an increase
235 in the ORP was observed with prolonged plasma-activation time ($P < 0.05$). Similar results were also
236 obtained in previous work (Guo et al., 2021; Tian et al., 2015; Xu et al., 2016; Xu et al., 2020). The
237 discharged gases in these previous works all contain oxygen, which is the same as our study. Hence, a
238 longer duration of plasma activation results in a larger amount of reactive oxygen species generated in
239 PAW and a high ORP value.

240 The pH values of PAW over the plasma-activated time were also measured (Fig. 1c). The pH value
241 of water after plasma activation decreased significantly ($P<0.05$) from 7.44±0.010 to 4.234±0.010.
242 However, after 45 min of plasma activation, the extended treatment time did not significantly influence
243 the pH values of PAW, which decreased over the plasma-activated time. Plasma discharge acidified
244 activated water (Oehmigen et al., 2010; Tian et al., 2015; Zhang et al., 2013; Xu et al., 2016). Due to the
245 discharge gases, some nitrate and nitrite were generated in PAW. Prolonged plasma activation
246 corresponds to larger amounts of hydrogen nitrate and nitrous acid, which lead to a lower pH value.

247 The electrical conductivity can indicate the concentrations of free ions present in an electrolytic
248 solution. The electrical conductivity of PAW was measured before and after plasma activation (Fig. 1d).
249 The conductivity of water after plasma activation increased from 2.3±0.3 μS cm^{-1} to 430.2±1.1 μS cm^{-1}.
250 The electrical conductivity of PAW increased in a plasma activation time-dependent manner, which
251 provided evidence for the accumulation of active ions in PAW. The results demonstrated that many active
252 ions were generated in PAW, which may be nitrate acid derived from chemical reactions between
253 electrons or RNS in cold plasma and water molecules (Guo et al., 2021; Ma et al., 2015).

However, the changes in ORP, pH and conductivity were not constant, which may be ascribed to the decomposition of ozone, reactive oxygen species and reactive nitrogen species (Guo et al., 2017; Guo et al., 2021; Shen et al., 2016).

3.2. In vivo fungicidal activities assay

To determine the fungicidal activities of PAW against FHB, the protection efficacies and disease severity indices were calculated. The symptoms caused by the pathogen were significantly reduced on the spikelets (Fig. 2). The pathogen treated by PAW generally failed to colonize the inoculated spikelets. The protection efficacies of PAW15, PAW30, PAW45 and PAW60 were 67.8%, 57.4%, 92.7% and 86.8%, respectively. Evaluations of disease development, which were quantified by calculating the disease severity index and the protection efficacy, revealed that PAW exhibited significant fungicidal activity ($P<0.05$) against FHB compared with the control.

The fungicides phenamacril, carbendazim and demethylation inhibitors are commonly used in the field. Compared to chemical synthetic fungicides, PAW has a similar protection efficacy (Chen et al., 2020; D'Angelo et al., 2014). The control efficacy of PAW in FHB increased with increasing the plasma activation time. In a previous study, there was a significant positive correlation between the ORP value and fungicidal activities. The half-value period of ORP in PAW stored inside was estimated to be approximately 9 days (Guo et al., 2021). The half-value period may decrease when PAW is used outdoors. Light can induce the acceleration of nitric acid dissipation of in PAW. The half-lives of phenamacril and carbendazim in soil were found to be 17.1 days and more than 28 days respectively (Donau et al., 2019; Huang et al., 2020). The half-lives of propiconazole and epoxiconazole varied between 20 and 130 days depending on the soil type (Hollomon, 2017). Therefore, in general, PAW has a shorter effective period

of antifungal activity than chemical synthetic fungicides.

3.3. Effect of PAW on mycelium growth, conidiation, conidium germination and total microbial activity

The results showed that the radial growth of *F. graminearum* was severely ($P < 0.05$) inhibited after PAW treatment (Fig. 3a). After 12 h of incubation, the mycelium length of PAW15-treated *F. graminearum* was 0.33±0.58 mm, whereas that of the control group was 1.56±0.43 mm. The mycelium length of *F. graminearum* did not increase after treatment with PAW30, PAW45, and PAW60. After incubation for 24 h, the radical growth of *F. graminearum* treated with PAW60 was still severely inhibited, but the mycelium lengths of the PAW45, PAW30, and PAW15 groups reached 1.46±0.44, 1.31±0.13, and 3.88±1.16 mm, respectively. After incubation for 36 h, a general increase in radial growth of *F. graminearum* treated with PAW60 was observed. Treatment with PAW led to an approximately 30% reduction in biomass production in comparison to untreated samples (Fig. 3b). The inhibition ratios of mycelium growth are shown in Fig. 3c. Twelve hours after treatment, the PAW30, PAW45, and PAW60 still demonstrated complete inhibition of mycelial growth. Twenty-four hours after treatment, only PAW60 completely inhibited mycelial growth. After 36 h of incubation, the inhibition ratio of mycelium growth in the PAW60 group decreased. These results were in line with those of previous studies showing that fungi were effectively inactivated as the plasma activation time increased (Ercan et al., 2013; Tian et al., 2015; Zhang et al., 2013; Ma et al., 2015). The results suggest that PAW treatment inhibited mycelial growth in a plasma-activated time-dependent manner.

PAW treatment could inhibit the germination of *F. graminearum* spores. The pH value of PAW decreased over plasma activation time. However, previous studies demonstrated that pH has no effect on *F. graminearum* germination (Beyer et al., 2004; Depasquale and Montville, 1990). Studies have

296 distinguished PAW-mediated inhibition from inhibition caused by pH alone, and the results have
297 suggested that the inhibitory effect on conidium germination was mainly due to the introduction of PAW.
298 The relative conidium germination ratios of *F. graminearum* treated with PAW15, PAW30, PAW45,
299 and PAW60 are shown in Fig. 3d. Similar results were reported after spores were treated with farnesol,
300 i.e., after 6 h, 44% of them failed to germinate (Semighini et al., 2008). The results of our study also
301 indicated that the antifungal activity of PAW increased over plasma activation time. The conidium
302 germination ratios of *F. graminearum* treated with PAW60 and PAW45 were significantly different from
303 that of control (P<0.01). Conversely, the conidium germination ratios of *F. graminearum* treated with
304 PAW30 and PAW15 were not significantly different from the control. The results were consistent with
305 the mycelium growth and conidiation assay findings. The inhibitory effect of PAW was time-specific
306 and increased over activation time.

307 Conidiation was measured after 7 days of culture on CM supplemented with 100 mg L^{-1}or 200 mg
308 L^{-1} Congo red and 50 mg L^{-1} Calcofluor White. As shown in Fig. 3e, the conidial production of PAW
309 treated strains was significantly ($P < 0.05$) reduced compared to that of the nontreated strains after 7
310 days of incubation. All the groups exhibited suppression of conidiation. The inhibitory effect increased
311 over the plasma activation time. PAW60 had the greatest inhibitory effect on the conidiation of *F.*
312 *graminearum*, and PAW15 had a weaker inhibitory effect on the conidiation than the other PAW
313 treatment. The results demonstrate that PAW could effectively suppress conidiation.

314 The total microbial activity of the spores was estimated through the fluorescein diacetate (FDA)
315 method. As shown in Fig. 4c, PAW-treated spores exhibited a decreased proportion of green fluorescence,
316 suggesting a decrease in the total microbial activity of spores after PAW treatments. This result was in
317 line with *in vitro* fungicidal activity assay.

318 The mode of PAW action in fungi is still subjected to thorough studies, but it has been suggested
319 that biological reactive substances such as ROS and RNS in PAW or cold plasma act synergistically in
320 microbial inactivation (Ercan et al., 2013; Los et al., 2020; Ma et al., 2015; Puligundla et al., 2018; Š
321 imončicová et al., 2018). The fungal cell wall and plasma membrane are the first cell structures that
322 collide with the radicals ROS and RNS in PAW. These reactive species could induce the oxidation of
323 glucose, (N-acetyl)-glucosamine, glycoproteins and glucan in the cell wall and lipid peroxidation in the
324 plasma membrane, causing membrane permeability changes, membrane damage, surface sculpturing in
325 cell wall, and eventually the direct exposure of intracellular components to reactive species. The SEM
326 and TEM results showed that spore cell wall and membrane sculpturing occurred after PAW treatment
327 (Fig. 4), supporting this hypothesis.

328 In addition to reactive species, the low pH can also inhibit hyphal growth (Wiebe et al., 1996). The
329 intracellular pH value plays an important role in the maintenance of normal cell function, and PAW can
330 cause significant acidification of the intracellular environment. Disruption of intracellular pH
331 homeostasis leads to irreversible cell damage (Lagadic-Gossmann et al., 2004; Xu et al., 2020). The
332 results indicated that acidification of the intracellular environment is mainly attributed to cell wall
333 damage and cell membrane dysfunction. A large amount of protons in PAW can directly enter *F.*
334 *graminearum* cells through damaged cell membranes.

335 *3.4. Effect of PAW on cell morphology and cell membrane integrity*

336 Morphological changes were observed in spores after PAW treatment (Fig. 4a and Fig. 4b). The cell
337 walls were intact in the control spores. No obvious morphological changes were present in the spores
338 treated with PAW15. Morphological changes were observed in the spores treated with PAW30, PAW45

339 and PAW60. The results from SEM and TEM observations in this study showed that PAW could cause
340 the surface sculpturing in the cell walls of spores, which may be attributed to the oxidative damage
341 induced by reactive species in PAW (Puligundla et al., 2018; Timoshkin et al., 2012; Xu et al., 2020). It
342 is generally agreed that ROS can lead to cell wall damage (Lu, et al., 2017; Shen et al., 2016; Xiang et
343 al., 2018; Xu et al., 2020). The composition of the cell wall, which includes glucose, (N-acetyl)-
344 glucosamine, glycoproteins and glucan, can be oxidized by these reactive species.

345 The cell membrane is an important organelle that maintains normal cell physiological metabolism.
346 In addition to cell wall damage, reactive species can cause changes in membrane permeability (Gaunt et
347 al., 2006). In this study, the FDA staining method and the DNA/RNA and protein leakage method were
348 employed to assess the effect of PAW on cell membrane integrity (Xiang et al., 2019a; Xu et al., 2020).

349 FDA easily entered the cell membranes and was cleaved by the enzymatic activity of nonspecific
350 esterase and, hence, was detected within live cells, and its fluorescence depends on cell membrane
351 integrity (Grimm et al., 2013; Jones et al., 2016). The decreased proportion of green fluorescence
352 indicated a defect in cell membrane integrity (Fig. 4c).

353 The leakage of intracellular DNA/RNA and proteins was also a significant indicator of the disruption
354 of cell membrane integrity. As shown in Table 1, upon the addition of PAW to *F. graminearum* spores,
355 there were no significant differences in absorbance (260 nm and 280 nm) in any of the treatment groups
356 compared with the control. Our results indicated that there was no leakage of DNA, RNA or protein, and
357 the cell membranes of the spores were not severely compromised by PAW.

358 In previous literature (Xiang et al., 2018; Xiang et al., 2019a), PAW treatment resulted in the leakage
359 of nucleic acids and proteins in *Pseudomonas deceptionensis* CM2 and *Escherichia coli* O157:H7, which
360 was not identical to our study, the leakage of intracellular DNA/RNA and proteins was not observed in

this work. The main reasons for this difference are probably attributed to the difference in membrane composition and the different ORP value of PAW. PAW can change the membrane permeability and allow small inorganic molecules such as RONS to enter the spore, but the extent of the change in membrane permeability was not sufficient to induce the leakage of biomacromolecules in this study.

3.5. Measurement of mitochondrial activity

The mitochondrial membrane potential ($\Delta\psi_m$) is an indicator of mitochondrial membrane integrity, and $\Delta\psi_m$ depolarizes when the membrane is perturbed, consequently combining with less TMRM probe. As shown in

Fig. 5 and Fig. S1**Error! Reference source not found.**, the fluorescence intensity of spores decreased significantly after PAW treatment, indicating that PAW could induce mitochondrial dysfunction, which is an important factor for *F. graminearum* inactivation by PAW. $\Delta\psi_m$ is essential for the survival of the cell as it drives the synthesis of ATP and maintains oxidative phosphorylation (Ly et al., 2003). Furthermore, the degree of depolarization of $\Delta\psi_m$ was in line with the ORP of PAW, and analysis of intracellular redox pairs such as NADH/NAD+ and GSH/GSSG indicated a correlation between extracellular ORP and intracellular redox homeostasis (Li et al., 2019). The existing literatures suggest that a significant increase of intracellular ROS could be induced by PAW (Ma et al., 2013; Tian et al., 2015; Xu et al., 2020). Based on these results, it is hypothesized that extracellular ORP leads to the accumulation of intracellular ROS, and ROS induce the opening of the mitochondrial permeability transition pore (mPTP), causing the depolarization of $\Delta\psi_m$ and mitochondrial dysfunction.

3.6. Overview of changes in gene expression of F. graminearum in response to PAW treatment

The numbers of clean reads for PAW-treated and untreated samples were 42,916,050±830015 and 39,063,536±918,515, respectively. The indicator Q30 value for PAW-treated and untreated samples were 94.15±0.15% and 94.37±0.07%, respectively. Uniquely mapped reads in the PAW-treated and -untreated libraries matched 82.49±1.88% and 87.20±1.76% of the total reads, respectively.

3.7. Differential gene expression analysis of F. graminearum strain PH-1 treated with PAW

Mapping of the raw RNA-seq expression data revealed that a total of 2837 (22%) of the 12,792 *F. graminearum* unigenes were differentially regulated by PAW treatment. The thresholds for differential expression were *P* adjusted < 0.001 and expression fold Change > 5 for up- and downregulated genes. By these criteria, we identified 703 genes upregulated and 676 genes downregulated by PAW. As shown in Fig. 6, of the 1379 genes, 944 genes were classified as having “unknown function”.

There were 3 putative genes (FGSG_10140, FGSG_04852, and FGSG_09329) involved in mitochondrial function in the 10 most upregulated genes and 1 gene (FGSG_03959) involved in the cell membrane in the top 5 downregulated genes in response to PAW. The results indicated that the cell membrane and mitochondria were the organelles most affected by PAW. Based on the results of this report and previous literatures, we mainly focused on the genes involved in mitochondrial function and cell wall and membrane integrity (Liu et al., 2010; Suwal et al., 2019; Los et al., 2020; Xu et al., 2020).

The most upregulated gene involved in mitochondrial function is listed in Table 3. The differences in gene expression of treated PH-1 ranged from up to a 3662.08-fold increase to a 11.35-fold increase compared to untreated PH-1. The most upregulated gene was FGSG_10140, and the putative product encoded by the gene is succinate dehydrogenase assembly factor. It is well known that succinate

401 dehydrogenase (complex II; or succinate: ubiquinone oxidoreductase, SQR) is a functional member of
402 the aerobic respiratory chain. Complex II couples the oxidation of succinate to fumarate in the
403 mitochondrial matrix with the reduction of ubiquinone in the membrane (Yankovskaya et al., 2003). It
404 was found that the SQR redox centers are arranged in a manner that aids the prevention of ROS formation
405 at the flavin adenine dinucleotide. This is likely to be the main reason FGSG_10140 and other genes are
406 highly expressed during PAW treatment, which can induce high intracellular ROS levels.

407 The top up- or downregulated genes involved in cell wall or membrane integrity are listed in Table
408 4. The differences in gene expression of treated PH-1 ranged from up to a 1731.37-fold increase to a
409 0.00049-fold decrease compared to untreated PH-1. The most upregulated gene was FGSG_02821, and
410 the putative product encoded by the gene is a transmembrane protein that belongs to the HPP family
411 according to NCBI BLAST analysis. These proteins are integral membrane proteins. While the function
412 of these proteins is uncertain, they may be transporters. It has been shown that the HPP family of integral
413 membrane proteins transports nitrite across the chloroplast membrane (Krapp, 2015; Maeda et al., 2014).
414 In addition, nitrate and nitrite exist in PAW generated by air plasma. Based on these results, it is
415 hypothesized that the FGSG_02821 gene is upregulated mainly in response to high nitrite or nitrate levels
416 in PAW.

417 The most downregulated gene was FGSG_03959, and the putative product encoded by the gene was
418 protein PTH11 according to NCBI BLAST analysis. PTH11 has been shown to be important for
419 appressorium formation and pathogenicity in *Magnaporthe grisea* (DeZwaan et al. 1999; Kou et al.,
420 2016). In addition, 30 genes were detected during infection of three hosts (wheat, barley, and maize)
421 encoding G-protein coupled receptors (GPCRs) belonging to the integral membrane protein PTH11 class,
422 and many exhibited host-preferential expression (Harris et al., 2016). As shown in Supplementary Table

1, 11 of the 30 genes showed differential expression during PAW treatment in our work, and 7 of the 11 genes were downregulated genes. Deletion of these downregulated genes resulted in a significant reduction in conidiation, confirming the result that PAW treatment reduces the conidiation of *F. graminearum*. However, the most downregulated gene, FGSG_03959, showed no or barely detectable expression in hyphae, perithecia and infected wheat heads during infection, indicating that the gene is probably not essential for plant infection (Jiang et al., 2019).

3.8. Validation of the differential expression results

In line with our main objective of identifying cell wall-, membrane integrity- or mitochondria-related genes, thirteen PH-1 unigenes were selected for further analysis on the basis of their expression levels and possible roles in defense mechanisms in response to PAW (Table 2). As shown in Table 5, in general, the Q-PCR results correlated with the transcriptomic data. However, the fold changes in expression determined by DESeq2 sequencing were not in line with those determined by Q-PCR. We observed that the expression levels of FGSG_10140, FGSG_04852, FGSG_09329, FGSG_06167, FGSG_08435, FGSG_05863 and FGSG_02821 determined by DESeq2 analysis were much higher than those determined by Q-PCR. The possible reason for these discrepancies is that the precision and accuracy of the methods are different.

4. Conclusion

In conclusion, the results from our study confirmed that PAW treatment is a highly effective disinfection procedure against *F. graminearum*. It has the potential to control fungal contamination. This study also unravels the potential antifungal mechanism of PAW from the perspective of cellular response

443 and differential gene expression. ROS and RNS in PAW first compromised the cell membrane, leading
444 to intracellular ROS accumulation, and then intracellular pH decreased, and depolarization of $\Delta\psi_m$ and
445 mitochondria dysfunction occurred. The DESeq2 sequencing analysis enhanced the hypothesis by the
446 fact that there were three putative genes involved in mitochondrial function in the 10 most upregulated
447 genes and one gene involved in the cell membrane in the top 5 downregulated genes in response to PAW
448 treatment. The information obtained from this work may verify the feasibility and validity of the
449 application of this technique in plant disease control and provides important insights into the antifungal
450 mechanism of PAW to fight against *F. graminearum*.

451 **Declaration of Competing Interest:**

452 The authors declare no conflict of interest in this paper.

453 **Acknowledgment**

454 The authors gratefully acknowledge the financial support provided by the National Natural Science
455 Foundation of China [grant number 31900126 to L. Li and 31701723 to J. Guo]; Zhejiang key research
456 and development program [grant number 2018C02G2011099]; and Program of Innovative
457 Entrepreneurship Training for Undergraduate of Zhejiang A & F University [grant number 2020KX0002,
458 2020KX0025].

459 **References**

460 Beyer, M., Röding, S., Ludewig, A., andVerreet J.A., 2004. Germination and survival of *Fusarium*
461 *graminearum* macroconidia as affected by environmental factors. J. Phytopathol. 152, 92–97.
462 https://doi.org/10.1111/j.1439-0434.2003.00807.x.

463 Bian, C.H., Duan,Y.H., Xiu, Q., Wang, J.Y., Tao, X., Zhou, M.G., 2021. Mechanism of validamycin A
464 inhibiting DON biosynthesis and synergizing with DMI fungicides against *Fusarium graminearum*.
465 Mol. Plant Pathol. In Press. https://doi.org/10.1111/mpp.13060.
466 Blandino, M., Minelli, L., Reyneri, A., 2006. Strategies for the chemical control fusarium head blight:
467 effect on yield, alveographic parameters and deoxynivalenol contamination in winter wheat grain.
468 Eur. J.Agron. 25, 193–201. https://doi.org/10.1016/j.eja.2006.05.001.
469 Brisset, J.L., Benstaali, B., Moussa, D., Fanmoe, J., Njoyim-Tamungang, E., 2011. Acidity control of
470 plasma-chemical oxidation: applications to dye removal, urban waste abatement and microbial
471 inactivation. Plasma Sources Sci. Technol. 20, 034021. https://doi.org/10.1088/0963-
472 0252/20/3/034021.
473 Chandana, L., Sangeetha, C.J., Shashidhar, T., Subrahmanyam, C., 2018. Non-thermal atmospheric
474 pressure plasma jet for the bacterial inactivation in an aqueous medium. Sci. Total Environ. 640,
475 493–500. https://doi.org/10.1016/j.scitotenv.2018.05.342.
476 Chen, Y., Yao, K., Wang, K., Xiao, C., Li, K., Khan, B., Zhao, S., Yan, W., Ye, Y., 2020. Bioactive-
477 guided structural optimization of 1,2,3-triazole phenylhydrazones as potential fungicides against
478 *Fusarium graminearum*. Pestic. Biochem. Phys. 164, 26–32.
479 https://doi.org/10.1016/j.pestbp.2019.12.004.
480 Cockrell, A. L., Fitzgerald, L. A., Cusick, K. D., Barlow, D. E., Tsoi, S. D., Soto, C. M., Baldwin, J.W.,
481 Dale, J.R., Morris, R.C., Little, B.J., Biffinger, J.C., 2017. A comparison of the physical and
482 biochemical properties of *Thermus scotoductus* SA-01 cultured with microwave radiation and
483 conventional heating. Appl. Environ. Microb. 81, 6285–6293. https://doi.org/10.1128/AEM.01618-
484 15.

485 Collos, Y., Mornet, F., Sciandra, A., Waser, N., Larson, A., Harrison, P.J., 1999. An optical method for
486 the rapid measurement of micromolar concentrations of nitrate in marine phytoplankton cultures. J.
487 Appl.Phycol. 11, 179–184. https://doi.org/10.1023/A:100804602.
488 D'Angelo, D.L., Bradley, C. A., Ames, K. A., Willyerd, K.T., Madden, L.V., Paul, P. A., 2014 Efficacy
489 of Fungicide Applications During and After Anthesis Against Fusarium Head Blight and
490 Deoxynivalenol in Soft Red Winter Wheat. Plant diease, 98, 1387–1397.
491 https://doi.org/10.1094/PDIS-01-14-0091-RE.
492 Demissie, A.Z., Foote, S.J., Tan, Y.F., Loewen, M.C., 2018 Profiling of the transcriptomic responses of
493 *Clonostachys rosea* upon treatment with *Fusarium graminearum* secretome. Front. Microbiol. 9,
494 1061. https://doi.org/10.3389/fmicb.2018.01061.
495 Depasquale, D.A., and Montville, T.J., 1990. Mechanism by which ammonium bicarbonate and
496 ammonium sulfate inhibit mycotoxigenic fungi. Appl. Environ. Microbiol. 56, 3711–3717.
497 https://doi.org/10.1002/bit.260361013.
498 DeZwaan, T.M., Carroll, A.M., Valent, B., Sweigard, J.A., 1999. Magnaporthe grisea Pth11p Is a Novel
499 Plasma Membrane Protein That Mediates Appressorium Differentiation in Response to Inductive
500 Substrate Cues. The Plant cell 11, 2013–2030. https://doi.org/10.1105/tpc.11.10.2013.
501 Donau, S.S., Bollmann, U.E., Wimmer, R., Bester, K., 2019. Aerobic dissipation of the novel
502 cyanoacrylate fungicide phenamacril in soil and sludge incubations. Chemosphere 233, 873–878.
503 https://doi.org/10.1016/j.chemosphere.2019.06.015.
504 Ercan, U.K., Wang, H., Ji, H.F., Fridman, G., Brooks, A.D., Joshi, S.G., 2013. Nonequilibrium plasma-
505 activated antimicrobial solutions are broad-spectrum and retain their efficacies for extended period
506 of time. Plasma Process. Polym. 10, 544−555. https://doi.org/10.1002/ppap.201200104.

507 Etzerodt, T., Gislum, R., Laursen, B.B., Heinrichson, K., Gregersen, P.L., Jorgensen, L.N., Fomsgaard,
508 I.S., 2016. Correlation of deoxynivalenol accumulation in *Fusarium*-infected winter and spring
509 wheat cultivars with secondary metabolites at different growth stages. J. Agric. Food Chem. 64,
510 4545−4555. https://doi.org/10.1021/acs.jafc.6b01162.
511 Gaunt, L.F., Beggs, C.B., Georghiou, G.E., 2006. Bactericidal action of the reactive species produced by
512 gas-discharge nonthermal plasma at atmospheric pressure: a review. IEEE Trans Plasma Sci 34,
513 1257– 1269. https://doi.org/10.1109/TPS.2006.878381.
514 Girard, P.M., Arbabian, A., Fleury, M., Bauville, G., Puech, V., Dutreix, M., Sousa, J.S., 2016.
515 Synergistic effect of H_2O_2 and NO_2 in cell death induced by cold atmospheric He plasma. Sci. Rep.
516 6, 29098. https://doi.org/10.1038/srep29098.
517 Gorbanev, Y., Privat-Maldonado, A., Bogaerts, A., 2018. Analysis of short-lived reactive species in
518 plasma–air–water systems: the dos and the do nots. Anal. Chem. 90, 13151–13158.
519 https://doi.org/10.1021/acs.analchem.8b03336.
520 Grimm, J.B., Heckman, L.M., Lavis, L.D., 2013. The chemistry of small-molecule fluorogenic probes.
521 Prog. Mol. Biol. Transl. 113, 1−34. https://doi.org/10.1016/B978-0-12-386932-6.00001-6.
522 Guo, J., Huang, K., Wang, X., Lyu, C., Yang, N., Li, Y., Wang, J., 2017. Inactivation of yeast on grapes
523 by plasma-activated water and its effects on quality attributes. J. Food Protect. 80, 225−230.
524 https://doi.org/10.4315/0362-028X.JFP-16-116.
525 Guo, J., Qin, D., Li, W., Wu, F., Li, L., Liu, X., 2021. Inactivation of P*enicillium italicum* on kumquat
526 via plasma-activated water and its effects on quality attributes. Int. J. Food Microbiol. 343, 109090.
527 https://doi.org/10.1016/j.ijfoodmicro.2021.109090.
528 Han, L., Patil, S., Boehm, D., Milosavljevic´, V., Cullen, P.J., Bourke, P., 2016. Mechanisms of

529 inactivation by high-voltage atmospheric cold plasma differ for *Escherichia coli* and
530 *Staphylococcus aureus*. Appl. Environ. Microbiol. 82 (2), 450–458.
531 https://doi.org/10.1128/AEM.02660-15.

532 Harris, L.J., Balcerzak, M., Johnston, A., Schneiderman, D., Ouellet, T., 2016. Host-preferential
533 Fusarium graminearum gene expression during infection of wheat, barley, and maize. Fungal Biol.
534 120, 111−123. https://doi.org/10.1016/j.funbio.2015.10.010.

535 Huang, T., Ding, T., Liu, D., Li J., 2020. Degradation of Carbendazim in Soil: Effect of Sewage Sludge-
536 Derived Biochars. J. Agric. Food Chem. 68, 3703–3710. https://doi.org/10.1021/acs.jafc.9b07244.

537 Itooka, K., Takahashi, K., Kimata, Y., Izawa, S., 2018. Cold atmospheric pressure plasma causes protein
538 denaturation and endoplasmic reticulum stress in *Saccharomyces cerevisiae*. Appl. Microbiol.
539 Biotechnol. 102 (5), 2279–2288. https://doi.org/10.1007/s00253-018-8758-2.

540 Jiang, C., Cao, S., Wang, Z., Xu, H., Liang, J., Liu, H., Wang, G., Ding, M., Wang, Q., Gong, C., Feng,
541 C., Hao, C., Xu, J., 2019. An expanded subfamily of G-protein-coupled receptor genes in *Fusarium*
542 *graminearum* required for wheat infection. Nat. Microbiol. 4, 1582–1591.
543 https://doi.org/10.1038/s41564-019-0468-8.

544 Jones, K., Kim, D.W., Park, J.S., Khang, C.H. 2016. Live-cell fluorescence imaging to investigate the
545 dynamics of plant cell death during infection by the rice blast fungus *Magnaporthe oryzae*. BMC
546 Plant Biol. 16, 69. https://doi.org/10.1186/s12870-016-0756-x.

547

548 Kaneko, T., Sasaki, S., Takashima, K., Kanzaki, M., 2017. Gas-liquid interfacial plasmas producing
549 reactive species for cell membrane permeabilization. J. Clin. Biochem. Nutr. 60, 3–11.
550 https://doi.org/10.3164/jcbn.16-73.

551 Kim, S.H., and Vujanovic, V., 2016. Relationship between mycoparasites lifestyles and biocontrol
552 behaviors against *Fusarium* spp. and mycotoxins production. Appl. Microbiol. Biotechnol. 100,
553 5257−5272. https://doi.org/10.1007/s00253-016-7539-z.
554 Kou, Y.J., Tan, Y.H., Ramanujam, R., Naqvi, N.I., 2016. Structure–function analyses of the Pth11
555 receptor reveal an important role for CFEM motif and redox regulation in rice blast. New Phytol.
556 24, 330−342. https://doi.org/10.1111/nph.14347.
557 Krapp, A., 2015. Plant nitrogen assimilation and its regulation: a complex puzzle with missing pieces.
558 Curr. Opin. Plant Biol. 25, 115–122. https://doi.org/10.1016/j.pbi.2015.05.010.
559 Lagadic-Gossmann, D., Huc, L., Lecureur, V., 2004. Alterations of intracellular pH homeostasis in
560 apoptosis: origins and roles. Cell Death Differ. 11, 953-961. https://doi.org/10.1038/sj.cdd.4401466.
561 Li, B. and Dewey, C.N., 2011. RSEM: accurate transcript quantification from RNA-Seq data with or
562 without a reference genome. BMC Bioinform. 12, 323. https://doi.org/10.1186/1471-2105-12-323.
563 Li, K., Xia, J., Muhammad Mehmood, A., Zhao, X.Q., Liu, C.G., Bai, F.W., 2019. Extracellular redox
564 potential regulation improves yeast tolerance to furfural. Chem. Eng. Sci. 196, 54−63.
565 https://doi.org/10.1016/j.ces.2018.11.059.
566 Liu, X., Jiang, J.H., Shao, J.F., Yin, Y.N., Ma Z.H., 2010. Gene transcription profiling of *Fusarium*
567 *graminearum* treated with an azole fungicide tebuconazole. Appl. Microbiol. Biotechnol. 85, 1105–
568 1114. https://doi.org/10.1007/s00253-009-2273-4.
569 Livak, K.J., and Schmittgen, T.D., 2001. Analysis of relative gene expression data using real-time
570 quantitative PCR and the 2–ΔΔCT method. Methods 25, 402–408.
571 https://doi.org/10.1006/meth.2001.1262.
572 Los, A., Ziuzina, D., Boehm, D., Cullen, P. J., Bourke, P., 2020. Inactivation efficacies and mechanisms

573 of gas plasma and plasma-activated water against *aspergillus flavus* spores and biofilms: a
574 comparative study. Appl. Environ. Microbiol. 86, e02619-19. https://doi.org/10.1128/AEM.02619-
575 19.

576 Lu, P., Boehm, D., Bourke, P., Cullen, P. J., 2017. Achieving reactive species specificity within plasma-
577 activated water through selective generation using air spark and glow discharges. Plasma
578 Process.Polym. 14, e1600207. https://doi.org/10.1002/ppap.201600207.

579 Lunov, O., Zablotskii, V., Churpita, O., Jäger, A., Polívka, L., Syková, E., Dejneka, A., Kubinová, Š.,
580 2016. The interplay between biological and physical scenarios of bacterial death induced by non-
581 thermal plasma. Biomaterials 82, 71–83. https://doi.org/10.1016/j.biomaterials.2015.12.027.

582 Ly, J.D., Grubb, D.R., Lawen, A., 2003. The mitochondrial membrane potential ($\Delta\psi_m$) in apoptosis; an
583 update. Apoptosis, 8, 115−128. https://doi.org/10.1023/a:1022945107762.

584 Lysøe, E., Pasquali, M., Breakspear, A., Kistler, H.C., 2011. The transcription factor FgStuAp influences
585 spore development, pathogenicity, and secondary metabolism in *Fusarium graminearum*. Mol.
586 Plant Microbe In. 24, 54−67. https://doi:10.1094/MPMI-03-10-0075.

587 Ma, R., Wang, G., Tian, Y., Wang, K., Zhang, J., Fang, J., 2015. Non-thermal plasma-activated water
588 inactivation of food-borne pathogen on fresh produce. J. Hazard. Mater. 300, 643−651.
589 http://doi.org/10.1016/j.jhazmat.2015.07.061.

590 Maeda S.I., Konishi M., Yanagisawa S., Omata T., 2014. Nitrite transport activity of a novel HPP family
591 protein conserved in cyanobacteria and chloroplasts. Plant Cell Phys. 55, 1311−1324.
592 https://doi.org/10.1093/pcp/pcu075.

593 Marcos, J.F., Munoz, A., Perez-Paya, E., Misra, S., Lopez-Garcia, B., 2008. Identification and rational
594 design of novel antimicrobial peptides for plant protection. Annu. Rev. Phytopathol. 46, 273−301.

595 http://doi.org/10.1146/annurev.phyto.121307.094843.

596 Masci, S., Laino, P., Janni, M., Botticella, E., Di Carli, M., Benvenuto, E., Danieli, P.P., Lilley, K.S.,
597 Lafiandra, D., D'Ovidio, R., 2015. Analysis of quality-related parameters in mature kernels of
598 polygalacturonase inhibiting protein (PGIP) transgenic bread wheat infected with *Fusarium*
599 *graminearum*.J. Agric. Food Chem. 63, 3962−3969. http://doi.org/10.1021/jf506003t.

600 McMullen, M., Jones, R., Gallenberg, D., 1997. Scab of wheat and barley: a re-emerging disease of
601 devastating impact. Plant Dis.81, 1340–1348. https://doi.org/10.1094/PDIS.1997.81.12.1340.

602 Mcferson, L.L., 1993. Understanding ORPS role in the disinfection process. Water-Eng. Manage. 140,
603 29−31.

604 Natali, M., Kamgang-Youbi, G., Herry, J.M., Bellon-Fontaine, M.N., Brisset, J.L., 2010. Combined
605 effects of long-living chemical species during microbial inactivation using atmospheric plasma-
606 treated water. Appl. Environ. Microbiol. 76, 7662−7664. http://doi.org/10.1128/AEM.01615-10.

607 Oehmigen, K., Hahnel, M., Brandenburg, R., Wilke, C., Weltmann, K.D., von Woedtke, T., 2010. The
608 role of acidification for antimicrobial activity of atmospheric pressure plasma in liquids. Plasma
609 Process. Polym. 7, 250−257. http://doi.org/10.1002/ppap.200900077.

610 Patangea, A., Lu, P., Boehm, D., Cullen, P.J., Bourke, P., 2019. Efficacy of cold plasma functionalised
611 water for improving microbiological safety of fresh produce and wash water recycling. Food
612 Microbiol. 84, 103226. https://doi.org/10.1016/j.fm.2019.05.010.

613 Pavlovich, M.J., Chang, H.W., Sakiyama, Y., Clark, D.S., Graves, D.B., 2013. Ozone correlates with
614 antibacterial effects from indirect air dielectric barrier discharge treatment of water. J. Phys. D: Appl.
615 Phys.46, 145202. https://doi.org/10.1088/0022-3727/46/14/145202.

616 Puligundla, P., Lee, T., Mok, C., 2018. Effect of intermittent corona discharge plasma treatment for

617 improving microbial quality and shelf life of kumquat (Citrus japonica) fruits. LWT-Food
618 Sci.Technol. 91, 8–13. https://doi.org/10.1016/j.lwt.2018.01.019.

619 Pimentel, D., Acquay, H., Biltonen, M., Rice, P., Silva, M., Nelson, J., Lipner, V., Giordano, S., Horowitz,
620 A., Damore, M., 1992. Environmental and economic costs of pesticide use. Bioscience 42, 750−760.
621 http://doi.org/10.2307/1311994.

622 Sarangapani, C., Danaher, M., Tiwari, B., Lu, P., Bourke, P., Cullen, P.J., 2017. Efficacy and mechanistic
623 insights into endocrine disruptor degradation using atmospheric air plasma. Chem. Eng. J. 326, 700–
624 714. https://doi.org/10.1016/j.cej.2017.05.178.

625 Semighini, C.P., Murray, N., Harris, S.D., 2008. Inhibition of *Fusarium graminearum* growth and
626 development by farnesol. FEMS Microbiol. Lett. 279, 259–264. https://doi.org/10.1111/j.1574-
627 6968.2007.01042.x.

628 Shen, J., Tian, Y., Li, Y., Ma, R., Zhang, Q., Zhang, J., Fang, J., 2016. Bactericidal effects against *S.*
629 *aureus* and physicochemical properties of plasma activated water stored at different temperatures.
630 Sci. Rep. 6, 28505. http://doi.org/10.1038/srep28505.

631 Šimončicová, J., Kaliňáková, B., Kováčik, D., Medvecká, V., Lakatoš, B., Kryštofová, S., Hoppanová,
632 L., Palušková, V., Hudecová, D., Ďurina, P., Zahoranováet, A., 2018. Cold plasma treatment
633 triggers antioxidative defense system and induces changes in hyphal surface and subcellular
634 structures of *Aspergillus flavus*. Appl. Microbiol. Biotechnol. 102, 6647–6658.
635 https://doi.org/10.1007/s00253-018-9118-y.

636 Soylu, E.M., Kurt, S., Soylu, S., 2010. In vitro and in vivo antifungal activities of the essential oils of
637 various plants against tomato grey mould disease agent Botrytis cinerea. Int. J. Food Microbiol.
638 143, 183–189. http://10.1016/j.ijfoodmicro.2010.08.015.

639 Suwal, S., Coronel-Aguileraa, C.P., Auer, J., Applegate, B., Garnerc, A.L., Huang, J., 2019. Mechanism
640 characterization of bacterial inactivation of atmospheric air plasma gas and activated water using
641 bioluminescence technology. Innov. Food Sci. Emerg. 53, 18–25.
642 https://doi.org/10.1016/j.ifset.2018.01.007.
643 Traylor, M.J., Pavlovich, M.J., Karim, S., Hait, P., Sakiyama, Y., Clark, D.S., Graves, D.B., 2011. Long-
644 term antibacterial efficacy of air plasma-activated water. J. Phys. D: Appl. Phys. 44, 472001.
645 http://doi.org/10.1088/0022-3727/44/47/472001.
646 Tian, Y., Ma, R.N., Zhang, Q., Feng, H.Q., Liang, Y.D., Zhang, J., Fang, J., 2015. Assessment of the
647 physicochemical properties and biological effects of water activated by non-thermal plasma above
648 and beneath the water surface. Plasma Process. Polym. 12, 439−449.
649 http://doi.org/10.1002/ppap.201400082.
650 Timoshkin, I.V., Maclean, M., Wilson, M.P., Given, M.J., MacGregor, S.J., Wang, T., Anderson, J.G.,
651 2012. Bactericidal effect of corona discharges in atmospheric air. IEEE Trans. Plasma Sci.40,
652 2322−2333. http://doi.org/10.1109/TPS.2012.2193621.
653 Wiebe, M.G., Robson, G.D., Oliver, S.G., Trinci, A.P.J., 1996. pH oscillations and constant low pH delay
654 the appearance of highly branched (colonial) mutants in chemostat cultures of the quorn® myco -
655 protein fungus, *Fusarium graminearum* A3/5. Biotechnol. Bioeng. 51, 61−68.
656 https://doi.org/10.1002/(SICI)1097-0290(19960705)51:1<61::AID-BIT7>3.0.CO;2-Z.
657 Xiang, Q., Kang, C., Niu, L., Zhao, D., Li, K., Bai, Y., 2018. Antibacterial activity and a membrane
658 damage mechanism of plasma activated water against *Pseudomonas deceptionensis* CM2. LWT-
659 Food Sci. Technol. 96, 395–401. http://doi.org/10.1016/j.lwt.2018.05.059.
660 Xiang, Q., Kang, C., Zhao, D., Niu, L., Liu, X., Bai, Y., 2019a. Influence of organic matters on the

661 inactivation efficacy of plasma-activated water against *E. coli* O157:H7 and *S. aureus*. Food Control,
662 99, 28–33. https://doi.org/10.1016/j.foodcont.2018.12.019.
663 Xiang, Q., Wang, W., Zhao, D., Niu, L., Li, K. Bai, Y., 2019b. Synergistic inactivation of *Escherichia*
664 *coli* O157:H7 by plasma-activated water and mild heat. Food Control, 106, 106741.
665 https://doi.org/10.1016/j.foodcont.2019.106741.
666 Xu, Y., Tian, Y., Ma, R., Liu, Q., Zhang, J., 2016. Effect of plasma activated water on the postharvest
667 quality of button mushrooms, *Agaricus bisporus*. Food Chem. 197, 436–444.
668 http://doi.org/10.1016/j.foodchem.2015.10.144.
669 Xu, H., Ma, R., Zhu, M., Du, M., Zhang, H., Jiao, Z., 2020. A systematic study of the antimicrobial
670 mechanisms of cold atmospheric-pressure plasma for water disinfection. Sci. Total Environ. 703,
671 134965. https://doi.org/10.1016/j.scitotenv.2019.134965.
672 Yankovskaya, V., Horsefield, R., Tornroth, S., Luna-Chavez, C., Miyoshi, H., Leger, C., Byrne, B.,
673 Cecchini, G., Lwata, S., 2003 Architecture of Succinate Dehydrogenase and Reactive Oxygen
674 Species Generation. Science 299, 700–704. https://doi.org/10.1126/science.1079605.
675 Zhang, Q., Liang, Y.D., Feng, H.Q., Ma, R.N., Tian, Y., Zhang, J., Fang, J., 2013. A study of oxidative
676 stress induced by non-thermal plasma-activated water for bacterial damage. Appl. Phys. Lett.102,
677 203701. http://doi.org/10.1063/1.4807133.
678 Zhang, Q., Ma, R., Tian, Y., Su, B., Wang, K., Yu, S., Zhang, J., Fang, J., 2016. Sterilization efficiency
679 of a novel electrochemical disinfectant against *Staphylococcus aureus*. Environ. Sci. Technol. 50,
680 3184–3192. http://doi.org/10.1021/acs.est.5b05108.
681 Zhou, Z.H., Duan, Y.B., Zhang, J., Lu, F., Zhu, Y.Y., Shim, W.B., Zhou, M.G., 2021. Microtubule-
682 assisted mechanism for toxisome assembly in *Fusarium graminearum*. Mol. Plant Pathol. 22, 163–

174. https://doi.org/10.1111/mpp.13015.

Zheng, Y.P., Wu, S.J., Dang, J., Wang, S.F., Liu, Z.X., Fang, J., Han, P., Zhang, J., 2019. Reduction of phoxim pesticide residues from grapes by atmospheric pressure non-thermal air plasma activated water. J. Hazard. Mater. 377, 98–105. https://doi.org/10.1016/j.jhazmat.2019.05.058.

687 Table 1 Release of intracellular nucleic acids and protein from spores treated with PAW.

Absorbance	Control	PAW15	PAW30	PAW45	PAW60
260 nm	0.098±0.003a	0.098±0.002a	0.095±0.006a	0.086±0.004b	0.087±0.003b
280 nm	0.054±0.002a	0.051±0.007a	0.043±0.003a	0.043±0.005a	0.044±0.004a

688 The results are expressed as the means ± standard deviations (n=6). Values with different letters in the
689 same row are significantly different ($P< 0.05$).
690

691 Table 2 A list of primers used in real-time PCR analysis

Target gene	Primer sequence (5'-3')
FGSG_10140	FGSG_10140-F1: ACCCCTCTCCACAACCGTTTCAC
	FGSG_10140-R1: GACTGGTAGACAAGGCGGGCTCG
FGSG_04852	FGSG_04852-F1: CGGCGATGGTGACAAGACTGAAG
	FGSG_04852-R1: ATGCTGGCGTCTTGACTGATTTC
FGSG_09329	FGSG_09329-F1: GATACCGATTTCCAGAAGAGCGT
	FGSG_09329-R1: GAACCAGGAGGACCAAGCACAGC
FGSG_06167	FGSG_06167-F1: CGCAAAACGAAGGACAACAACCC
	FGSG_06167-R1: GGCTTCGGTAGTGGGATGTTTGA
FGSG_08435	FGSG_08435-F1: CTGTCGCACCCTCACCAAGAACC
	FGSG_08435-R1: GATGACGGGTCCAGGCGAGTTAC
FGSG_05863	FGSG_05863-F2: CTGTGTGGTCTTTGATGCGTGGA
	FGSG_05863-R2: TCCGATGGGGTGTGCTCTTCTTC
FGSG_07299	FGSG_07299-F2: CGAATGTGACGACAAAAGATGGA
	FGSG_07299-R2: CATCAACCTCAATCAAATACGCC
FGSG_01743	FGSG_01743-F2: CGACACTGTTCTGATTGACCCCG
	FGSG_01743-R2: CCAGTGAAGTAGTATCCAGGGTA
FGSG_05401	FGSG_05401-F1: TACGGATACCGCACATCTTTGGA
	FGSG_05401-R1: GCCCATCCTTTGGTAAACCCCGT
FGSG_02821	FGSG_02821-F1: TCATCAATCCCTTCATTCCACCG
	FGSG_02821-R1:GAAGGTATGCGTTCTGAAGCCAA
FGSG_09830	FGSG_09830-F1: AAGATGGCTCTCCAAATCGCTAT
	FGSG_09830-R1: CGAGACCGAAAGGAGCGGAGTAG
FGSG_04144	FGSG_04144-F2: TCAAGTCCATTCCAAAGGTCATC
	FGSG_04144-R2: ACCATTCTTTGGCAGTTCTCGTA
FGSG_03959	FGSG_03959-F1: TCATCGTGTCATTTTGCTTCGGT
	FGSG_03959-R1: ATGTCATCTTGAATGTCTTGGGC
FGSG_07335 (Actin)	Actin-F ATCCACGTCACCACTTTCAA
	Actin-R TGCTTGGAGATCCACATTTG

692

693 Table 3 Response to PAW of the genes involved in mitochondrial function

Accession number	Putative product encoded by the gene	Fold change in gene expression[a]	Padjust
FGSG_10140	Hypothetical protein similar to succinate dehydrogenase assembly factor 2, mitochondrial	3662.08	<0.001
FGSG_04852	Hypothetical protein similar to NADH-cytochrome b5 reductase	2195.27	<0.001
FGSG_09329	Hypothetical protein similar to ATPase	2122.66	<0.001
FGSG_06167	Hypothetical protein similar to 54s ribosomal protein L4, mitochondrial	839.12	<0.001
FGSG_08435	Hypothetical protein similar to nitronate monooxygenase	783.80	<0.001
FGSG_05863	Mitochondrial import protein 1	714.07	<0.001
FGSG_07299	Hypothetical protein similar to transferase CAF17, mitochondrial	37.54	<0.001
FGSG_01743	Acetyl-coenzyme A synthetase	11.35	<0.001

694 [a]Fold-change value represents the fold expression in *F. graminearum* treated with PAW as compared to
695 that in nontreatment control
696

697 Table 4 Response to PAW of the genes involved in cell wall and membrane integrity

Accession number	Putative product encoded by the gene	Fold change in gene expression[a]	Padjust
FGSG_02821	Hypothetical protein similar to transmembrane protein	1731.37	<0.001
FGSG_04144	Hypothetical protein similar to vi polysaccharide biosynthesis vipa tvib	47.51	<0.01
FGSG_05401	Hypothetical protein similar to Beta-1,3-glucanase	12.46	<0.001
FGSG_09830	C-4 methylsterol oxidase	9.60	<0.001
FGSG_03959	Hypothetical protein similar to plasma membrane protein pth11	0.00049	<0.001

698 [a]Fold-change value represents the fold expression in *F. graminearum* treated with PAW as compared to
699 that in nontreatment control
700

701 Table 5 Comparison in the changes of gene expression determined by DESeq2 sequencing and real-time

702 PCR approaches

Accession number	Putative product encoded by the gene	Fold change in gene expression determined by DESeq2 sequencing[a]	Fold change in gene expression determined by real-time PCR[a]
FGSG_10140	Hypothetical protein similar to succinate dehydrogenase assembly factor 2, mitochondrial	3662.08	52.83
FGSG_04852	Hypothetical protein similar to NADH-cytochrome b5 reductase	2195.27	40.41
FGSG_09329	Hypothetical protein similar to ATPase	2122.66	2.52
FGSG_06167	Hypothetical protein similar to 54s ribosomal protein L4, mitochondrial	839.12	14.32
FGSG_08435	Hypothetical protein similar to nitronate monooxygenase	783.80	22.12
FGSG_05863	Mitochondrial import protein 1	714.07	12.64
FGSG_07299	Hypothetical protein similar to transferase CAF17, mitochondrial	37.54	2.18
FGSG_01743	Acetyl-coenzyme A synthetase	11.35	19.47
FGSG_02821	Hypothetical protein similar to transmembrane protein	1731.37	7.95
FGSG_04144	Hypothetical protein similar to vi polysaccharide biosynthesis vipa tvib	47.51	7.13
FGSG_05401	Hypothetical protein similar to Beta-1,3-glucanase	12.46	10.90
FGSG_09830	C-4 methylsterol oxidase	9.60	13.48
FGSG_03959	Hypothetical protein similar to plasma membrane protein pth11	0.00049	0.080

703 [a]Fold-change value represents the fold expression in *F. graminearum* treated with PAW as compared to
704 that in nontreatment control
705
706

Figure captions

Fig. 1 Physicochemical properties of PAW: a) Concentrations of nitrate anions (NO_3^-) (□) and nitrite anions (NO_2^-)(△) in PAW. b) ORP value of PAW subjected to plasma activation for 0, 15, 30, 45, and 60 min. c) pH value of PAW subjected to plasma activation for 0, 15, 30, 45, and 60 min. d) Conductivity of PAW subjected to plasma activation for 0, 15, 30, 45, and 60 min. The results represent the mean±standard deviation (n=3). Vertical bars represent standard deviation of the mean, columns with different letters represent statistically significant results ($P < 0.05$).

Fig. 2 Disease severity indexes are the mean area of disease divided by the total area of the wheat × 100%. Groups of bars followed by the same letter are not significantly different according to Fisher's protected least significant difference ($P < 0.05$).

Fig. 3 a) Representative image of the colony morphology of *F. graminearum* exposed to PAW15, PAW30, PAW45, and PAW60 treatment for 1h; an image was obtained every 12 h after treatment with PAW during 5 days of incubation at 28 °C. b) Dry mycelial weight after PAW treatment cultured in CM supplemented with 100 mg L^{-1}, 200 mg L^{-1} Congo red and 50 mg L^{-1} Calcofluor White. c) Inhibition ratio of mycelium growth after treatment with PAW during 5 days of incubation at 28 °C on CM plate. d) Conidium germination ratio and relative conidium germination ratio of *F. graminearum* after treatment with PAW cultured in CM. R: conidium germination ratio, R_e: relative conidium germination ratio. e) Conidiation of *F. graminearum* treated with PAW after 7 days culture in CM supplemented with 100 mg L^{-1}, 200 mg L^{-1} Congo red and 50 mg L^{-1} Calcofluor White. The results represent the mean±standard deviation (n=6). Vertical bars represent standard deviation of the mean, columns with different letters represent statistically significant results ($P < 0.05$).

728 Fig. 4. a) SEM images of spores treated with PAW. b) TEM images of spores treated with PAW. c) The

729 fluorescence images of *F. graminearum* spores stained by FDA.

730 Fig. 5. The fluorescence images of *F. graminearum* spores stained by TMRM.

731 Fig. 6 COG categories of differentially expressed genes relative to PAW-treated *F. graminearum*.

732

733 **Highlights:**

734 • The viability of F. graminearum is notably inhibited by PAW

735 • The symptoms caused by *F. graminearum* were significantly reduced on the spikelets

736 • Oxidative stress induce cell wall sculpturing, membrane permeability change

737 • PAW can cause the mitochondrial dysfunction

738 • Cell wall, membrane and mitochondria are the most affected organelles by PAW

739

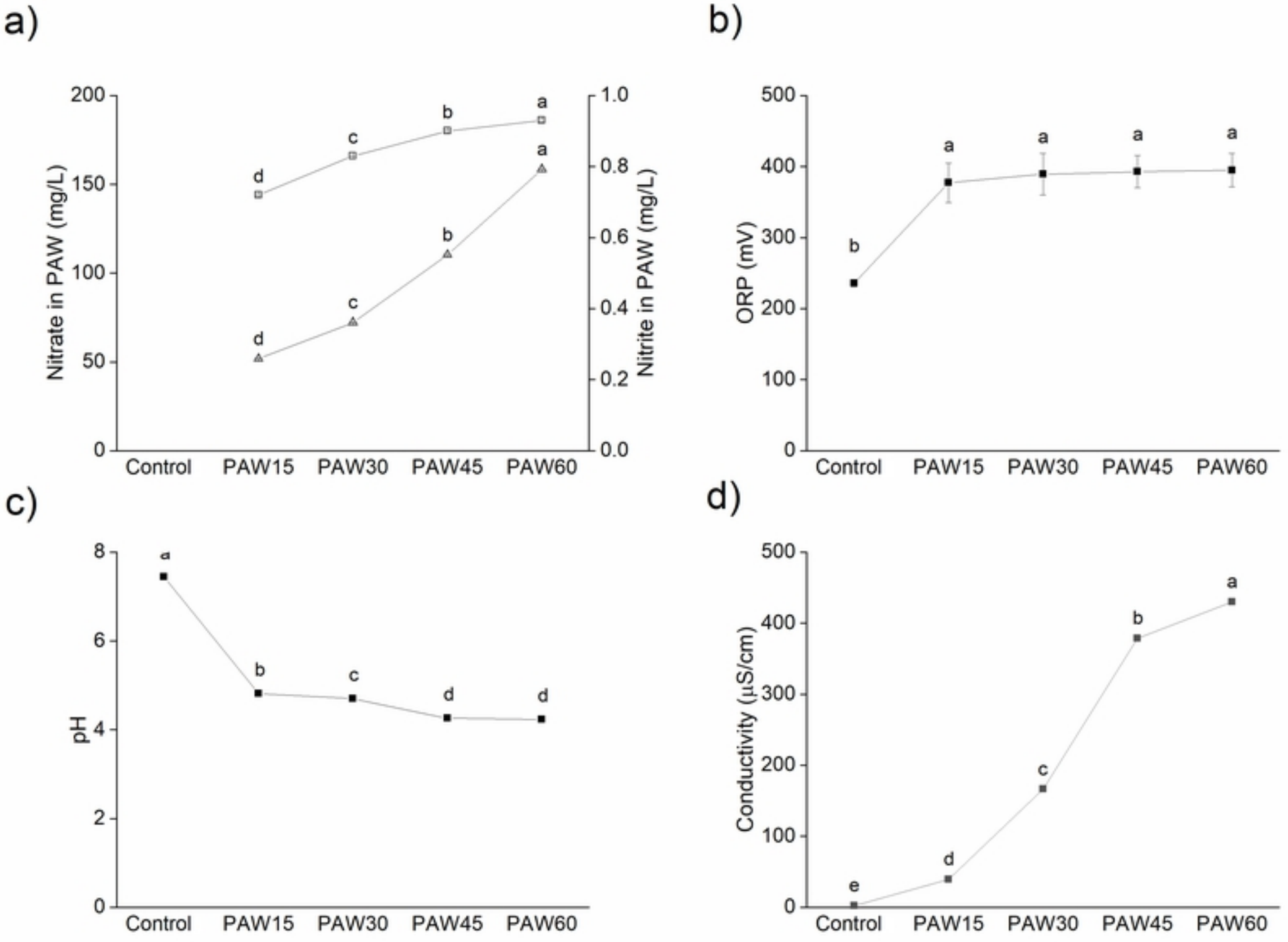
a)
Nitrate in PAW (mg/L)
Nitrite in PAW (mg/L)
200
150
100
50
0
1.0
0.8
0.6
0.4
0.2
0.0
d
c
b
a
d
c
b
a
Control
PAW15
PAW30
PAW45
PAW60
b)
ORP (mV)
500
400
300
200
100
0
b
a
a
a
a
Control
PAW15
PAW30
PAW45
PAW60
c)
pH
8
6
4
2
0
a
b
c
d
d
Control
PAW15
PAW30
PAW45
PAW60
d)
Conductivity (μS/cm)
500
400
300
200
100
0
e
d
c
b
a
Control
PAW15
PAW30
PAW45
PAW60

Figure1

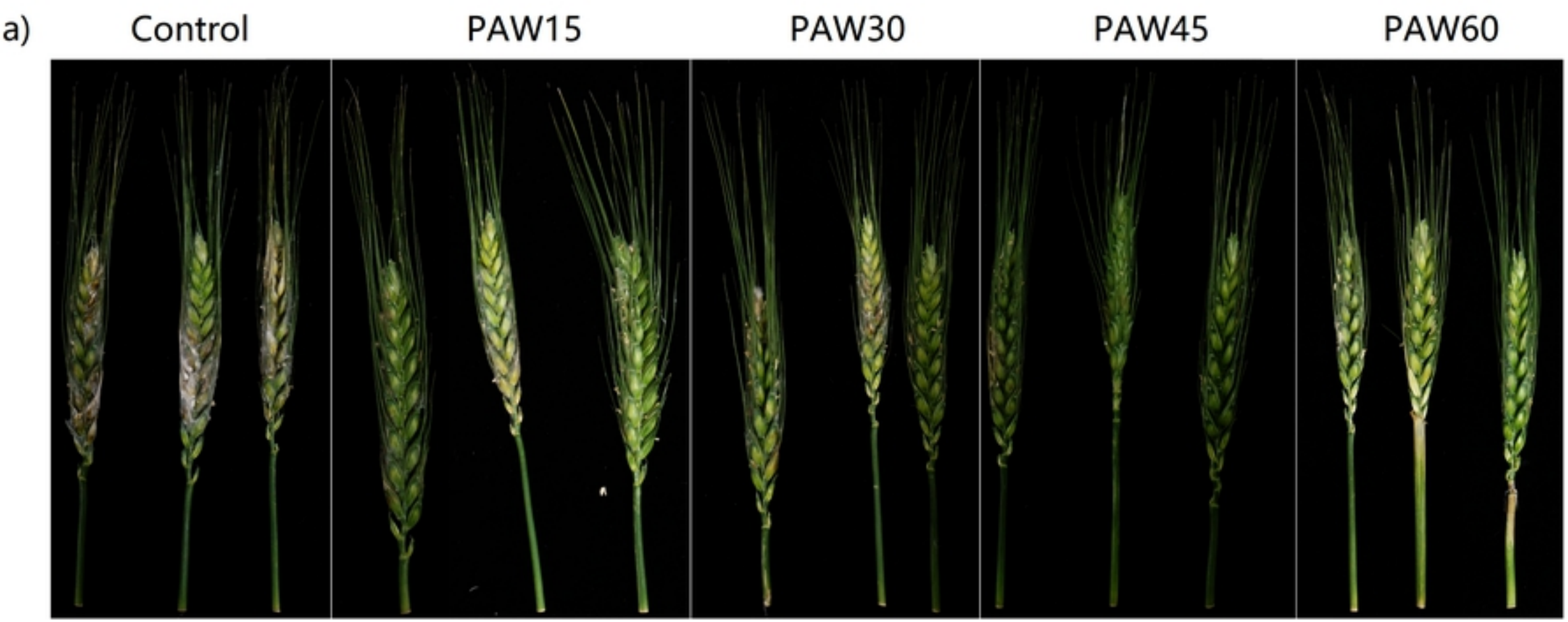

Figure2a

b)

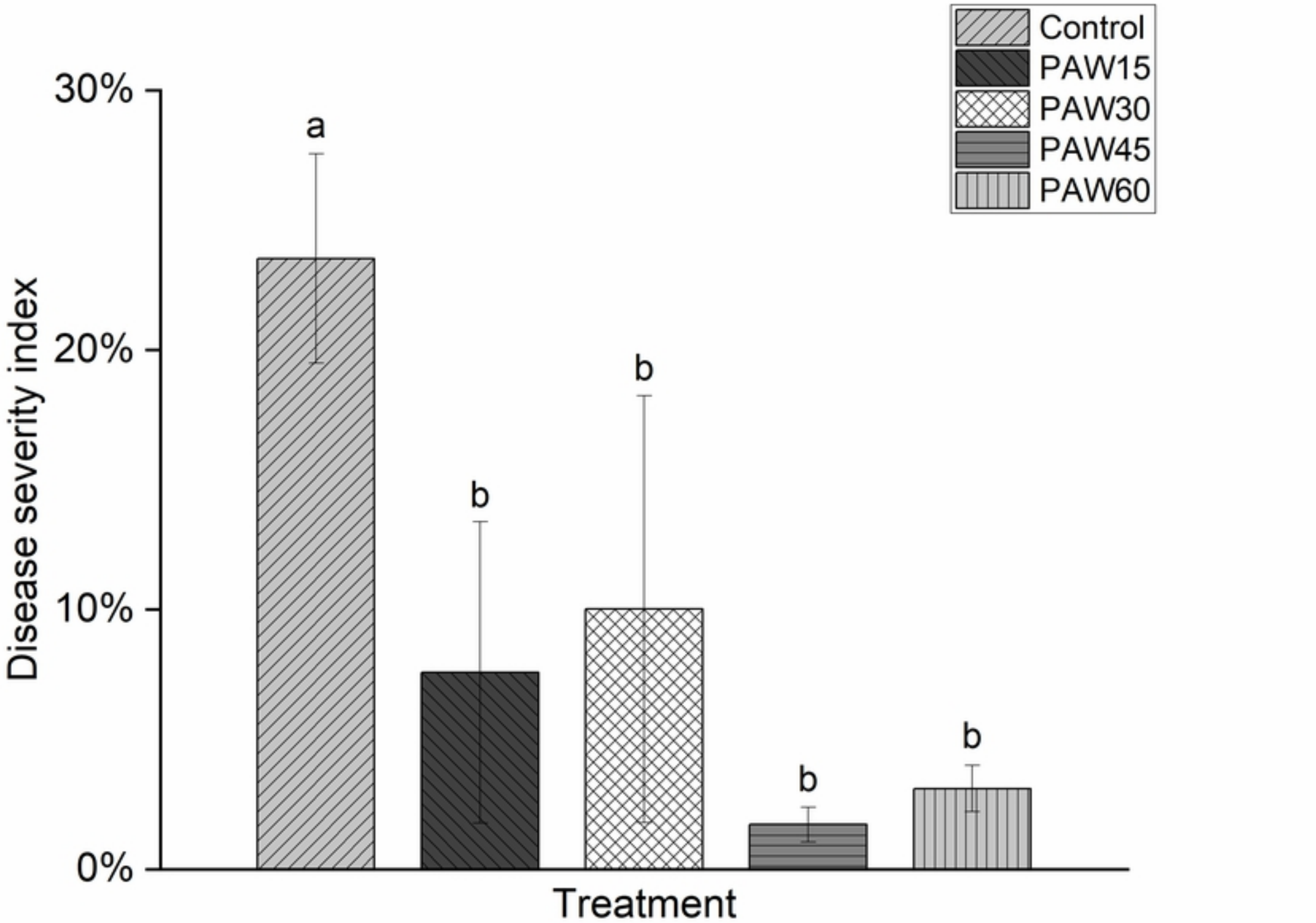
Control
PAW15
PAW30
PAW45
PAW60
30%
20%
10%
0%
Disease severity index
a
b
b
b
b
Treatment

Figure2b

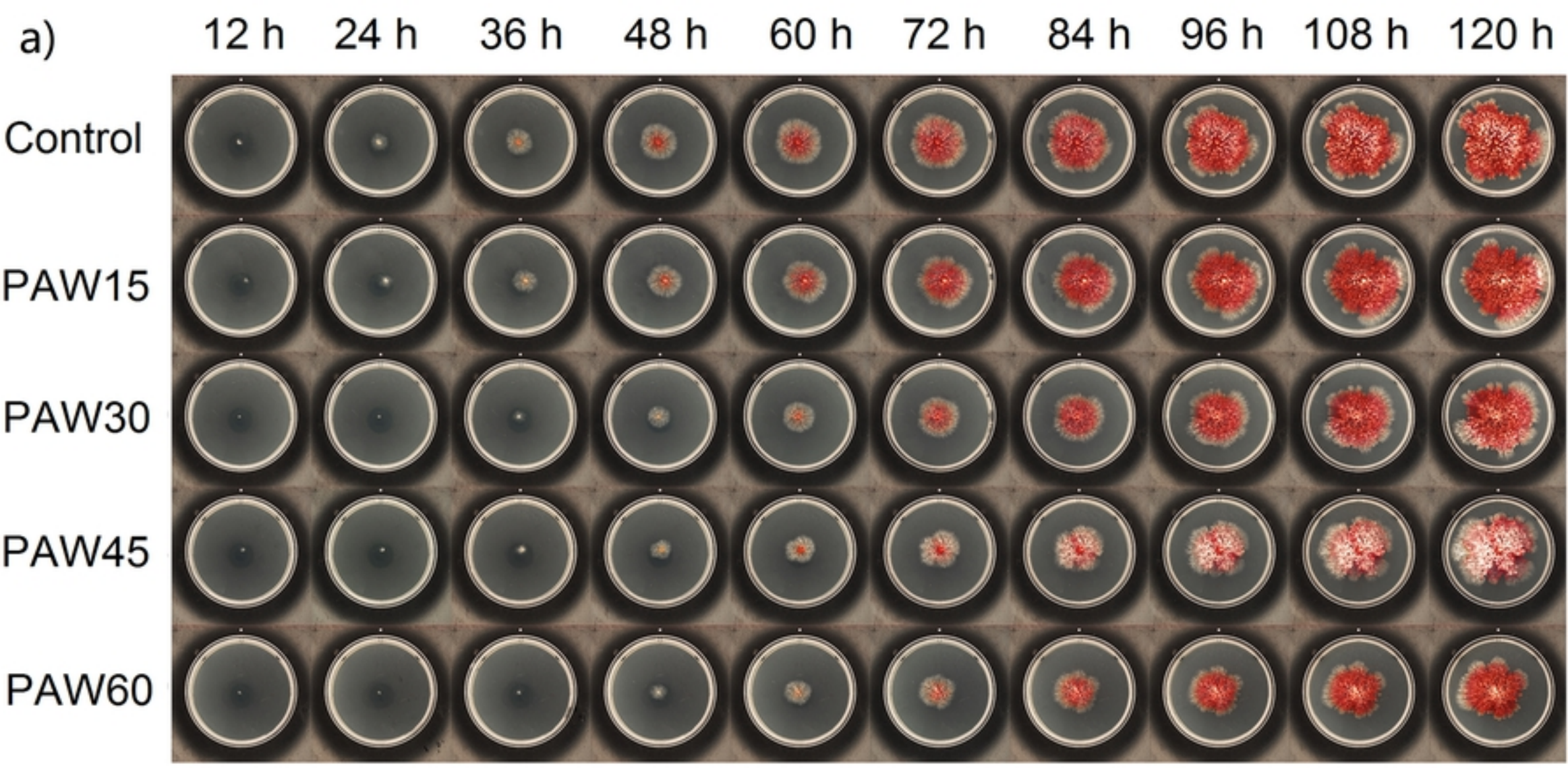
a)
12 h
24 h
36 h
48 h
60 h
72 h
84 h
96 h
108 h
120 h
Control
PAW15
PAW30
PAW45
PAW60

Figure3a

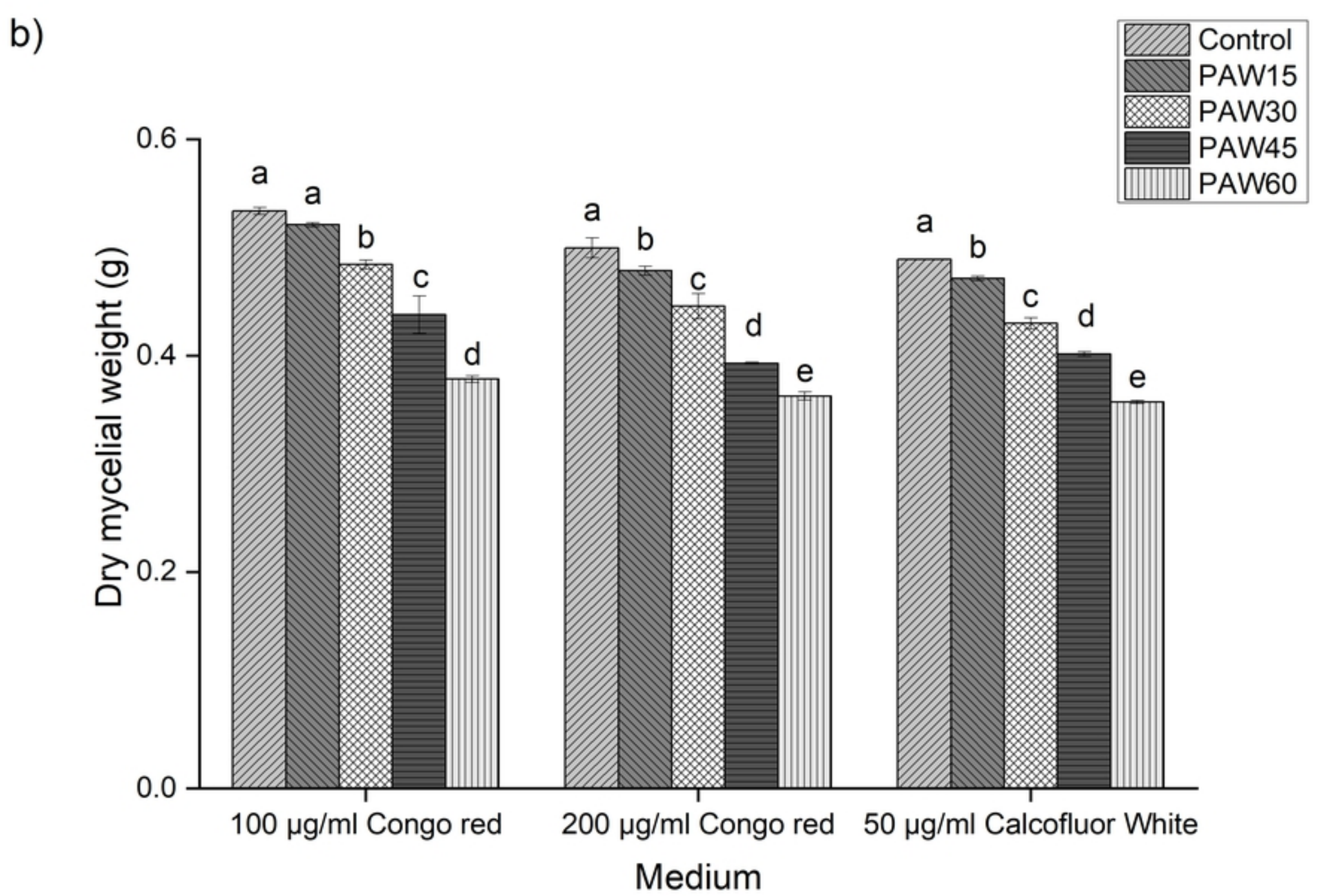
b)
Control
PAW15
PAW30
PAW45
PAW60
Dry mycelial weight (g)
0.6
0.4
0.2
0.0
a
a
b
c
d
a
b
c
d
e
a
b
c
d
e
100 µg/ml Congo red
200 µg/ml Congo red
50 µg/ml Calcofluor White
Medium

Figure3b

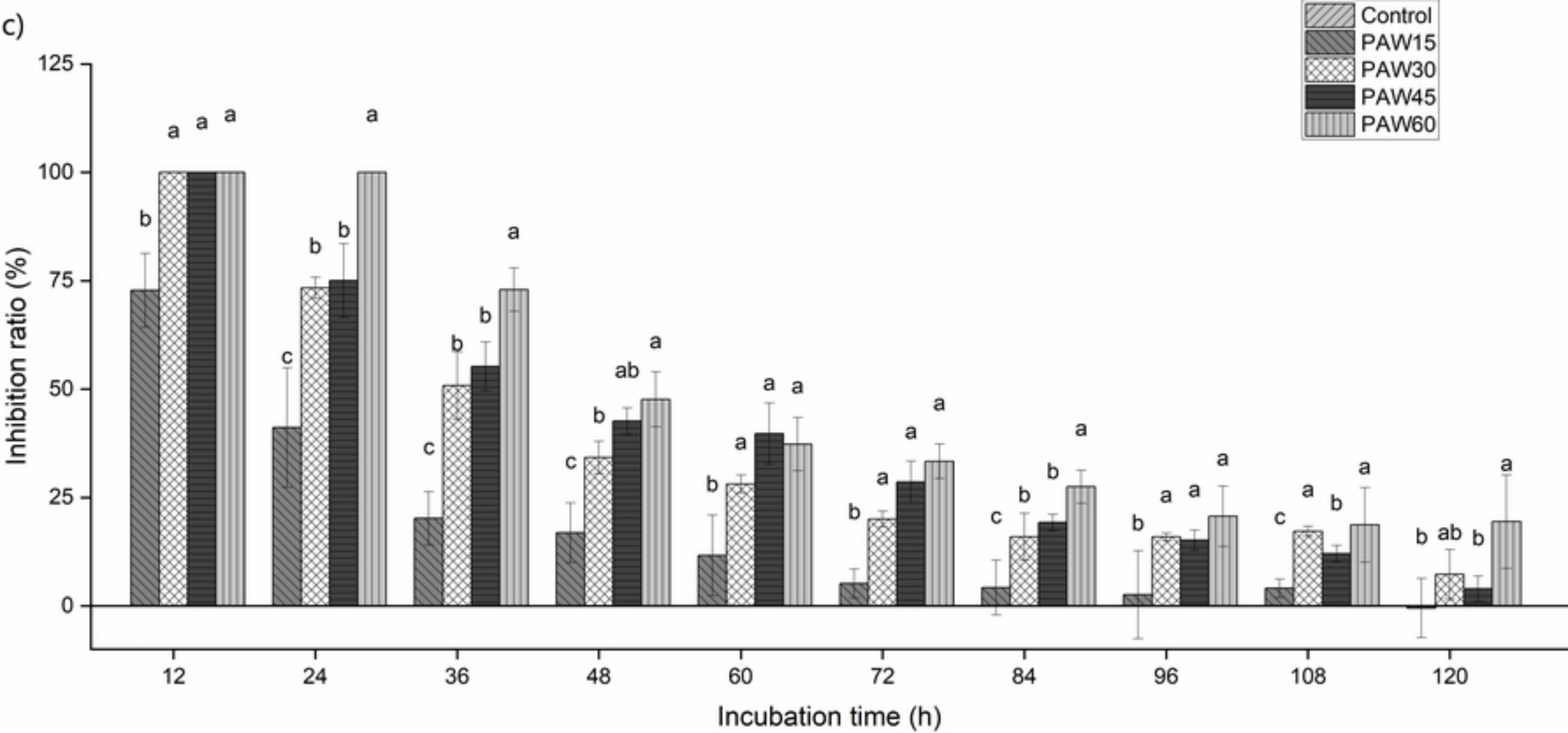
c)
Control
PAW15
PAW30
PAW45
PAW60
Inhibition ratio (%)
125
100
75
50
25
0
12
24
36
48
60
72
84
96
108
120
Incubation time (h)

Figure3c

d)

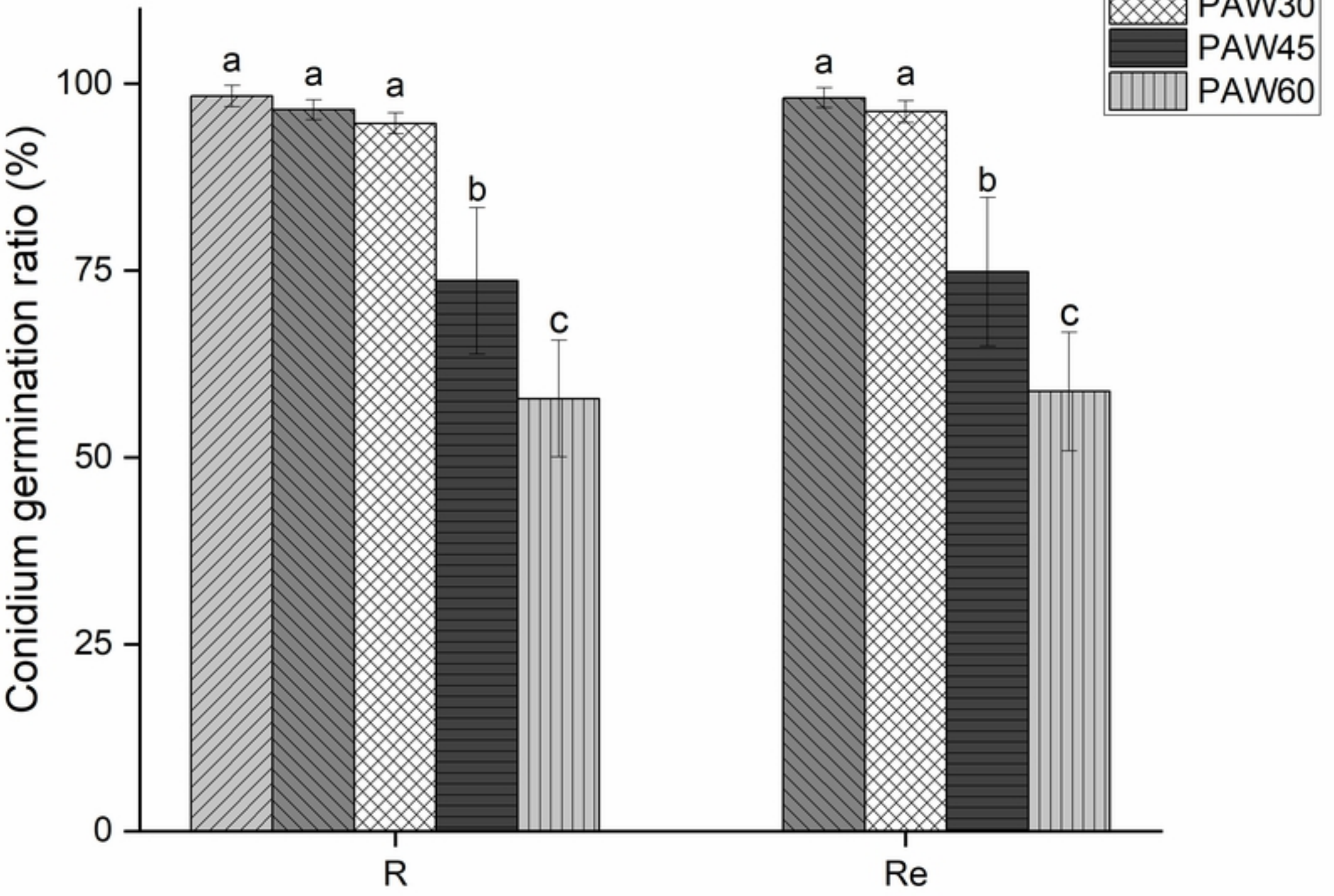
Control
PAW15
PAW30
PAW45
PAW60
Conidium germination ratio (%)
100
75
50
25
0
a
a
a
b
c
a
a
b
c
R
Re

Figure3d

e)

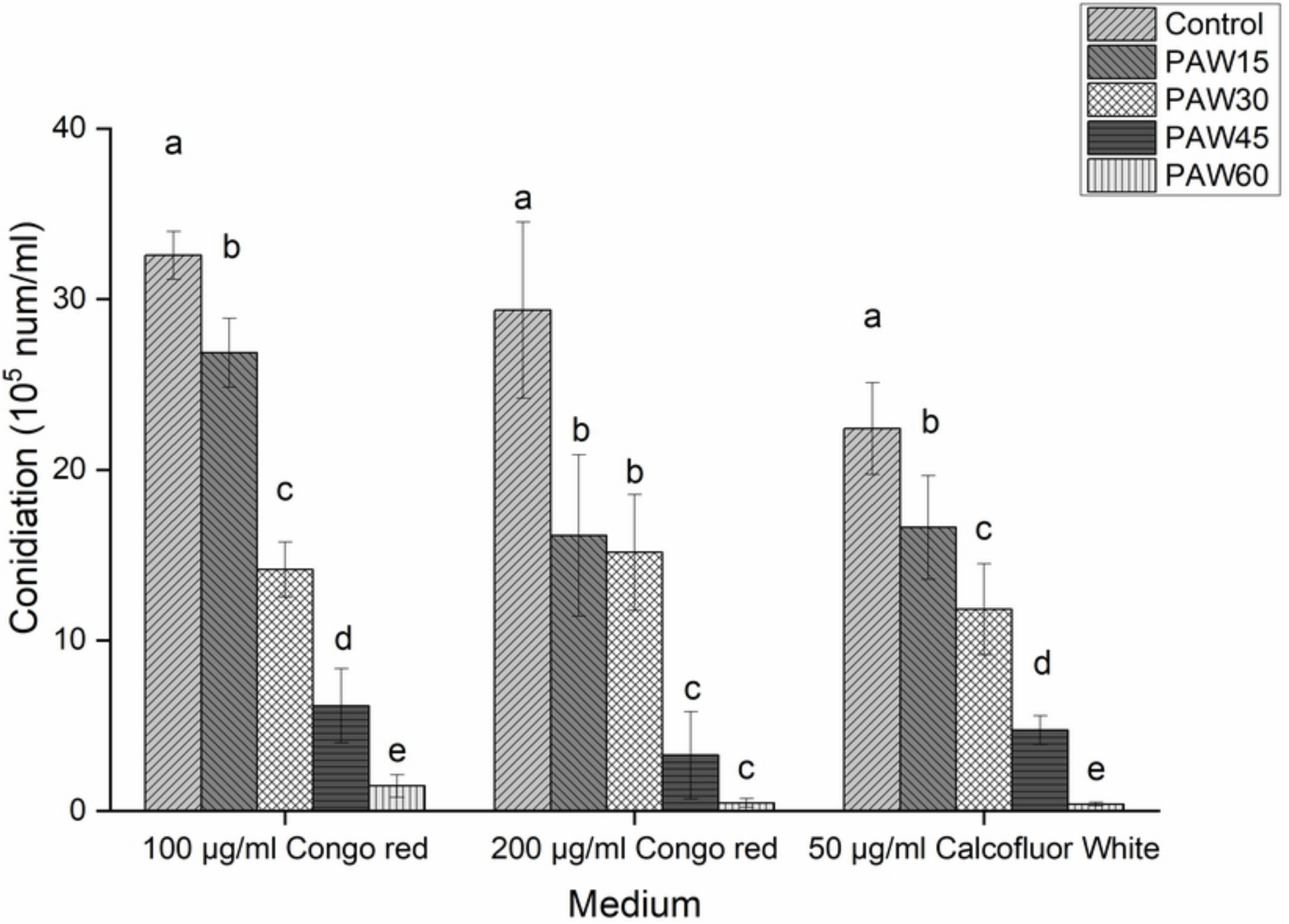
Control
PAW15
PAW30
PAW45
PAW60
Conidiation (10^5 num/ml)
40
30
20
10
0
a
b
c
d
e
a
b
b
c
c
a
b
c
d
e
100 µg/ml Congo red
200 µg/ml Congo red
50 µg/ml Calcofluor White
Medium

Figure3e

Figure4a

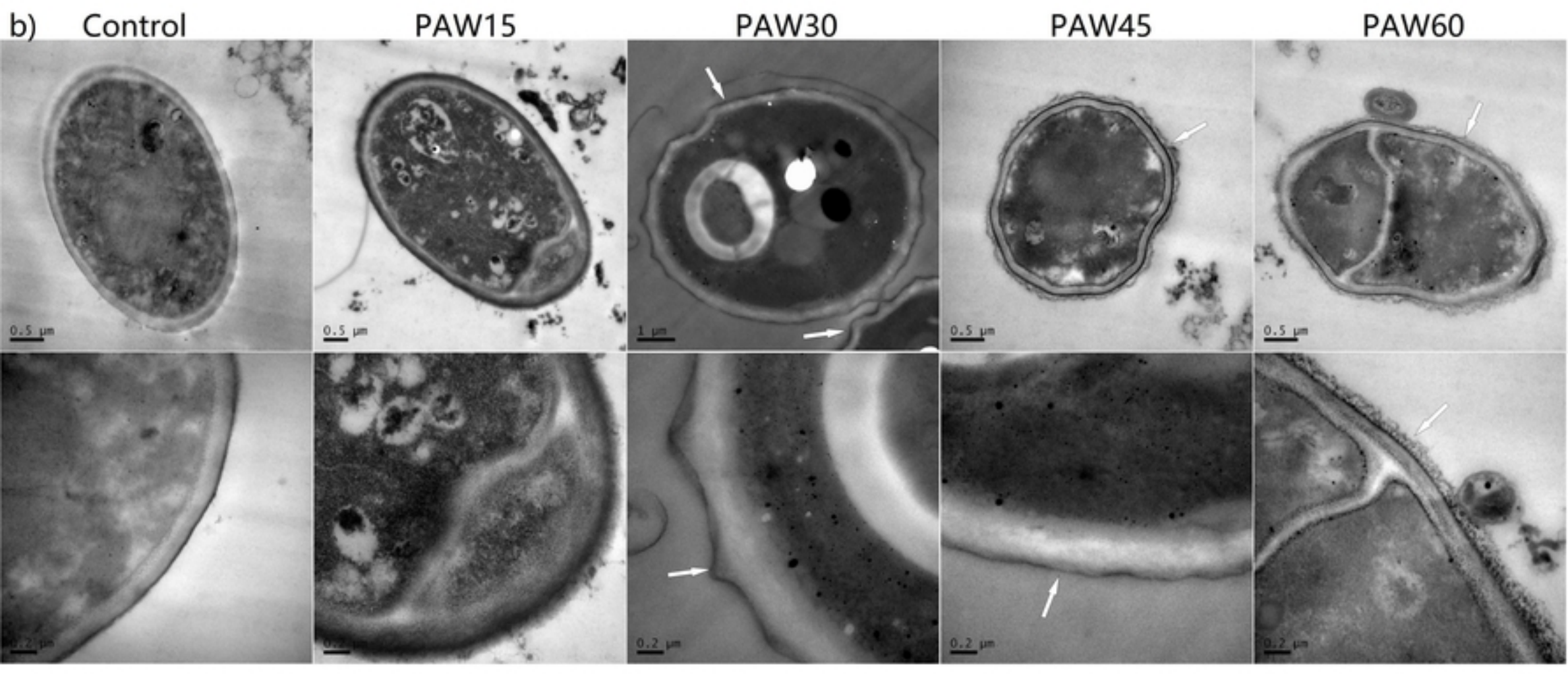
b)
Control
PAW15
PAW30
PAW45
PAW60
0.5 µm
0.5 µm
1 µm
0.5 µm
0.5 µm
0.2 µm
0.2 µm
0.2 µm

Figure4b

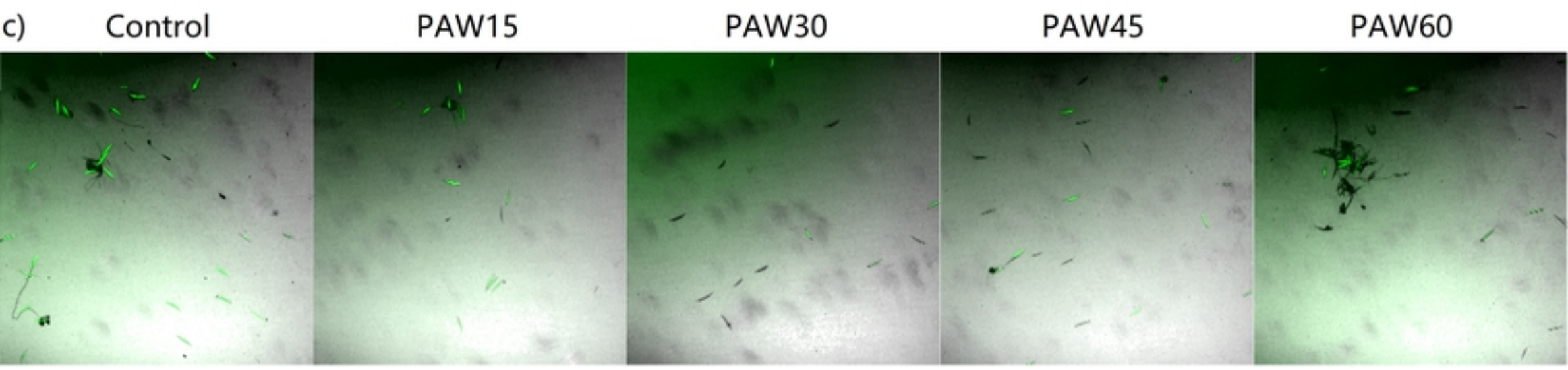

Figure4c

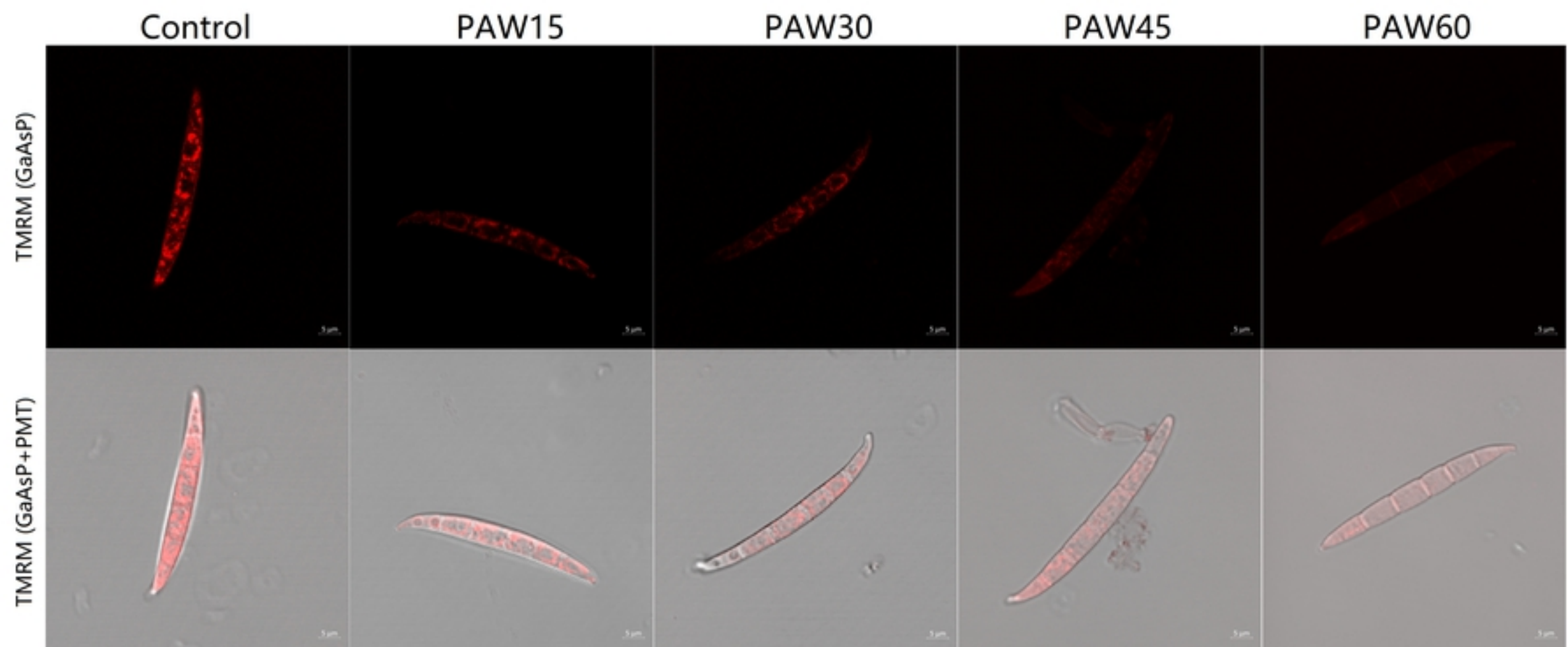

Figure5

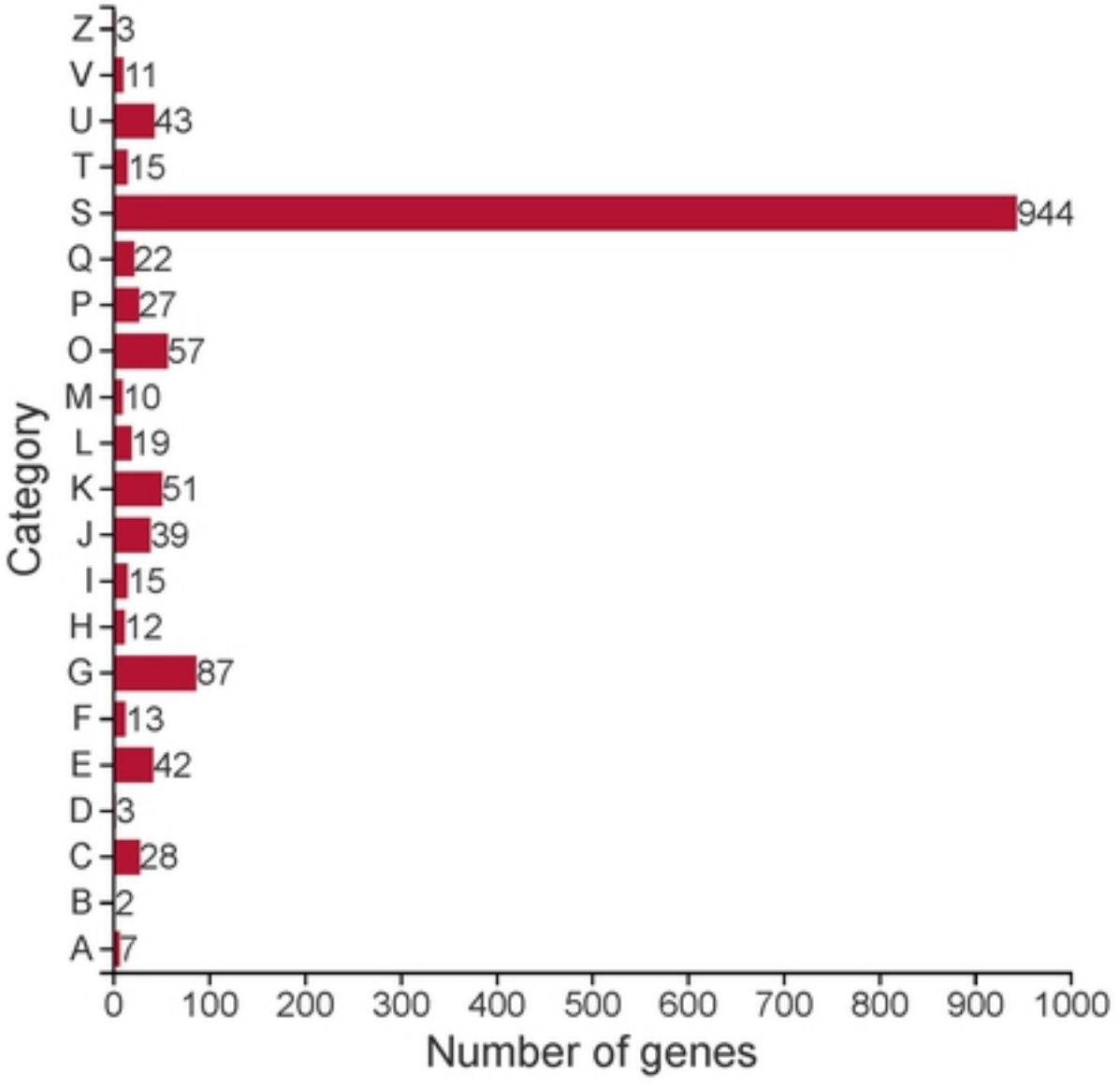

A: RNA processing and modification
B: Chromatin structure and dynamics
C: Energy production and conversion
D: Cell cycle control, cell division, chromosome partitioning
E: Amino acid transport and metabolism
F: Nucleotide transport and metabolism
G: Carbohydrate transport and metabolism
H: Coenzyme transport and metabolism
I: Lipid transport and metabolism
J: Tanscription, ribosomal structure and biogenesis
K: Transcription
L: Replication, recombination and repair
M: Cell wall/membrane/envelope biogenesis
O: Posttranslational modification, protein turnover, chaperones
P: Inorganic ion transport and metabolism
Q: Secondary metabolites biosysnthesis, transport and catabolism
S: Function unknown
T: Signal transduction mechanisms
U: Intracellular trafficking, secretion, and vesicular transport
V: Defense mechanisms
Z: Cytroskeleton

Figure6